

INFORMATION TO USERS

This manuscript has been reproduced from the microfilm master. UMI films the text directly from the original or copy submitted. Thus, some thesis and dissertation copies are in typewriter face, while others may be from any type of computer printer.

The quality of this reproduction is dependent upon the quality of the copy submitted. Broken or indistinct print, colored or poor quality illustrations and photographs, print bleedthrough, substandard margins, and improper alignment can adversely affect reproduction.

In the unlikely event that the author did not send UMI a complete manuscript and there are missing pages, these will be noted. Also, if unauthorized copyright material had to be removed, a note will indicate the deletion.

Oversize materials (e.g., maps, drawings, charts) are reproduced by sectioning the original, beginning at the upper left-hand corner and continuing from left to right in equal sections with small overlaps.

**ProQuest Information and Learning
300 North Zeeb Road, Ann Arbor, MI 48106-1346 USA
800-521-0600**

UMI[®]

**THE FLORIDA STATE UNIVERSITY
COLLEGE OF ARTS AND SCIENCES**

**AN OPEN BOUNDARY CONDITION FOR LAYER TO LEVEL OCEAN MODEL
INTERACTION**

By

ANDREA C. MASK

**A Dissertation submitted to the
Department of Oceanography
in partial fulfillment of the
requirements for the degree of
Doctorate of Philosophy**

**Degree Awarded:
Fall Semester, 2002**

UMI Number: 3076197

UMI[®]

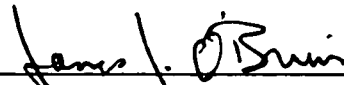
UMI Microform 3076197

Copyright 2003 by ProQuest Information and Learning Company.

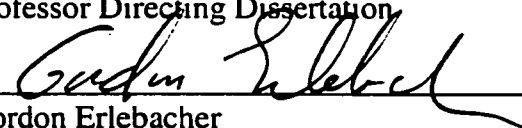
All rights reserved. This microform edition is protected against
unauthorized copying under Title 17, United States Code.

ProQuest Information and Learning Company
300 North Zeeb Road
P.O. Box 1346
Ann Arbor, MI 48106-1346

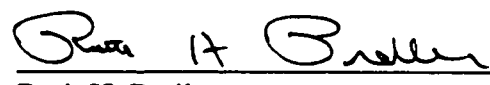
The members of the Committee approve the dissertation of Andrea C. Mask defended on
October 9, 2002.




James J. O'Brien
Professor Directing Dissertation




Gordon Erlebacher
Outside Committee Member



Ruth H. Preller
Committee Member



Richard Iverson
Committee Member



Georges Weatherly
Committee Member

ACKNOWLEDGEMENTS

This research was conducted under “Ocean Modeling and Prediction” grant N00173-01-2-C901. I would first like to thank Dr. James J. O’Brien for this continuous support, and equally Dr. Ruth H. Preller at NRL – Stennis Space Center whose encouragement and guidance were invaluable.

At FSU, I would also like to acknowledge Drs. Mark Bourassa and Steve Morey, who willingly listened to the struggles along the way and offered help when they could.

At NRL – Stennis Space Center, I would like to acknowledge many, many people, but I will try to keep the list short. First Alan Wallcraft and Paul Martin, for their developmental work on the models used in this study and their help in using and modifying the model code. Next, Dr. John Kindle whose previous work with normal mode calculations was very helpful. Also, Dr. Peter Rochford whose interest in my topic provided many stimulating conversations. Finally, Deanna Chappell whose friendship was a blessing, who willingly listened when things were not going well.

Last, but not least, to my husband, Chris, and daughter, Tatiana, who have struggled along side me. Thank you!

TABLE OF CONTENTS

List of Tables	v
List of Figures	vi
Abstract	viii
1. INTRODUCTION	1
2. NORMAL MODE BOUNDARY CONDITION BASICS	6
2.1 Model Formulation	6
2.2 Normal Mode Open Boundary Conditions	8
2.3 Numerical Example	10
3. NUMERICAL TESTS	21
3.1 Gaussian Perturbation – Nested NCOM	21
3.2 Gaussian Perturbation – Coupled NCOM	25
3.3 Gaussian Perturbation – NLOM Coupled to NCOM	36
4. CONCLUSIONS	47
5. FUTURE WORK	49
APPENDIX A	50
APPENDIX B	55
APPENDIX C	60
REFERENCES	62
BIOGRAPHICAL SKETCH	65

LIST OF TABLES

1. Density calculation input and results rounded to the nearest thousandths. CM is the coarse mesh calculation. FM is the fine mesh calculation. T is the potential temperature. S is the salinity. σ is the density.	12
2. Square Brünt-Väisälä frequencies (N^2) calculated by the model. CM is the coarse mesh values. FM is the fine mesh values.	14
3. Calculated values of the coefficients from equation (19) where the diagonals are the coefficients for p_q and the subdiagonals are the coefficients for p_{q-1}	15
4. Calculated eigenvectors and their corresponding phase speeds. Recall mode number 0 corresponds to the barotropic mode, and mode numbers 1 – 12 are the baroclinic modes.	16
5. The barotropic (mode=0) and first three baroclinic normal modes. CM is the coarse mesh and FM is the fine mesh.	17
6. Modal components of salinity upon application of equation (11) where the mean salinity value has been subtracted. CM is the coarse mesh results. FM is the fine mesh results.....	18
7. The direction of propagation calculated from the sign of the results of equation (15). Direction equal to 0.0 results in propagation into the fine mesh. Direction equal to 1.0 results in propagation out of the fine mesh. CM is the coarse mesh results. FM is the fine mesh results.	19
8. Modal Salinity after the radiation condition has been applied and the combining of the fine and the coarse mesh solutions is completed. Final Salinity is the result of applying the inverse of equation (11) and adding back the mean salinity value.	20

LIST OF FIGURES

1. Z-grid showing positions of N^2 and p . p is given at the locations marked with a dot, and N^2 is located at points marked with and x.	13
2. Salinity results of the CM NCOM for days 0, 15, and 30, with contours of the NMOBC salinity result in the left column and contours of the Orlanski results in the right column. FM bounding box is in gray. Contours match the color-scale interface values.	23
3. U-Velocity results of the CM NCOM for days 0.25, 15, and 30, with contours of the NMOBC salinity result in the left column and contours of the Orlanski results in the right column. FM bounding box is in gray. Contours match the color-scale interface values.	24
4. Difference plot for level 3 U-Velocity of the coarse mesh NCOM run at the fine mesh resolution and the NMOBC solution for the coupled NCOM to NCOM fine mesh at days 10, 20, 30, and 40.	26
5. Difference plot for level 3 V-Velocity of the coarse mesh NCOM run at the fine mesh resolution and the NMOBC solution for the coupled NCOM to NCOM fine mesh at days 10, 20, 30, and 40.	27
6. Difference plot for level 3 Salinity of the coarse mesh NCOM run at the fine mesh resolution and the NMOBC solution for the coupled NCOM to NCOM fine mesh at days 10, 20, 30, and 40.	28
7. Difference plot for level 3 U-Velocity of the coarse mesh NCOM run at the fine mesh resolution and the Orlanski solution for the coupled NCOM to NCOM fine mesh at days 10, 20, 30, and 40.	29
8. Difference plot for level 3 V-Velocity of the coarse mesh NCOM run at the fine mesh resolution and the Orlanski solution for the coupled NCOM to NCOM fine mesh at days 10, 20, 30, and 40.	30
9. Difference plot for level 3 Salinity of the coarse mesh NCOM run at the fine mesh resolution and the Orlanski solution for the coupled NCOM to NCOM fine mesh at days 10, 20, 30, and 40.	31

10: Time series plot of salinity along the equator of the coarse mesh domain run with the fine mesh resolution (left), NCOM-NCOM coupling with Orlanski boundary conditions (middle), and NCOM-NCOM coupling with NMOBC's.	32
11: Time series plot of salinity along 132°W of the coarse mesh domain run with the fine mesh resolution (left), NCOM-NCOM coupling with Orlanski boundary conditions (middle), and NCOM-NCOM coupling with NMOBC's.	33
12. Difference plot for level 3 U-Velocity of the coarse mesh NCOM run at the fine mesh resolution and the NMOBC solution for the coupled NLOM to NCOM fine mesh at days 10, 20, 30, and 40.	39
13. Difference plot for level 3 V-Velocity of the coarse mesh NCOM run at the fine mesh resolution and the NMOBC solution for the coupled NLOM to NCOM fine mesh at days 10, 20, 30, and 40.	40
14. Difference plot for level 3 Salinity of the coarse mesh NCOM run at the fine mesh resolution and the NMOBC solution for the coupled NLOM to NCOM fine mesh at days 10, 20, 30, and 40.	41
15. Difference plot for level 3 U-Velocity of the coarse mesh NCOM run at the fine mesh resolution and the Orlanski solution for the coupled NLOM to NCOM fine mesh at days 10, 20, 30, and 40.	42
16. Difference plot for level 3 V-Velocity of the coarse mesh NCOM run at the fine mesh resolution and the Orlanski solution for the coupled NLOM to NCOM fine mesh at days 10, 20, 30, and 40.	43
17. Difference plot for level 3 Salinity of the coarse mesh NCOM run at the fine mesh resolution and the Orlanski solution for the coupled NLOM to NCOM fine mesh at days 10, 20, 30, and 40.	44
18: Time series plot of u-velocity along the equator of the coarse mesh domain run with the fine mesh resolution (left), NLOM-NCOM coupling with Orlanski boundary conditions (middle), and NLOM-NCOM coupling with NMOBC's.	45
19: Time series plot of u-velocity along 132°W of the coarse mesh domain run with the fine mesh resolution (left), NLOM-NCOM coupling with Orlanski boundary conditions (middle), and NLOM-NCOM coupling with NMOBC's.	46
20. Bottom topography of coarse mesh grid proposed for future work. Inner box represents location of proposed fine mesh.	48

ABSTRACT

A radiation open boundary condition based on vertical normal modes is introduced. This boundary condition has been applied to both a nested and a coupled Equatorial Kelvin wave propagation test using the Naval Research Laboratory Coastal Ocean Model (NCOM), which is a sigma-z-level hybrid coordinate model. This boundary condition has also been applied to the more computationally difficult problem of coupling the Naval Research Laboratory Layered Ocean Model (NLOM), which is an isopycnal coordinate model, to the NCOM for the test case.

The NCOM is a primitive equation ocean model which employs the hydrostatic, Boussinesq, and incompressible approximations and uses a free surface. The NLOM is a primitive equation ocean model, which is hydrodynamic (isopycnal) and utilizes a free surface. Because both of these models use the full primitive equations, vertical normal mode theory shows that the form of the modal equations is identical for the two models in the linear limit. This allows a physical linkage between the two models that can be used in a boundary condition application that is advanced in many ways over standard radiation boundary condition approaches.

This approach is shown to be superior to standard radiation open boundary conditions in NCOM coupling tests in which the number of vertical levels in the forcing domain are fewer than the number of vertical levels in the area of interest. The superiority comes both in the reduction of reflected outgoing waves, and in the ability to

recognize and adjust the differences in the physics, of the two models, that affect wave speed. An advantage to the latter superiority is that the noise created by the numerics of the boundary condition and the error created by the differences in the physics of the two models are distinct from each other. Another advantage is that the forcing data does not need to be vertically interpolated at any time to be used in this calculation, thus reducing one source of numerical noise or error.

The lack of vertical interpolation and the use of a physically motivated linkage are advantages over numerical techniques when the forcing model uses different physical equations than the model used to investigate an area of interest.

1. INTRODUCTION

Ocean models allow oceanographers to explore ocean physics without the expense and time of scientific voyages but with the added benefit of denser data coverage. Yet, modeling is not without monetary and time expense. As the base of ocean knowledge expands, models with finer and finer resolution are desired to investigate smaller and smaller ocean features. Because even small-scale dynamics are influenced by the basin scale dynamics of the ocean, it quickly becomes expensive to run a model of an ocean area of interest and all of its forcing area at the desired grid resolution and time step.

Two techniques for handling the computational expense of modeling small-scale ocean dynamics are coupling and nesting. Coupling uses data saved from a previous integration of a basin scale model at a course grid resolution and time scale to force a fine grid resolution model of the area of interest. Nesting links the basin scale and fine scale models as the models run simultaneously. There are two types of nesting one-way (passive), where only the fine grid is influenced in the interaction and two-way (interactive), where both models influence each other. The key to either coupling or nesting successfully lies in the handling of the communication between the grids. The communication between the grids must not only handle the passing of forcing information, but also control potential noise created at the artificial interface by

reflections of improperly specified waves trying to cross the boundary. The purpose of this paper is to describe a new technique, which can be used for either nesting or coupling ocean models. This paper will focus on passing information without interpolation of vertical grid information yet allow the coarse and fine grids to have different vertical structure.

Atmospheric models were the first to use nesting as an approach to solve primitive-equations in domains of differing horizontal resolutions. Interactive nests use separation of the dynamic and mesh interface (Kurihara et al, 1979) among other techniques to reduce noise at the nest interface. A summary of atmospheric techniques appears in Zhang et al. (1986). One of the first uses of interactive nested models in oceanography was reported by Spall and Holland (1991). Fox and Maskell (1995) expanded Spall and Holland's work from increased resolution in the horizontal only to increased resolution in the vertical and horizontal. Most interactive nesting methods are founded on the idea of designing an interpolation scheme to transfer information from a global or large-scale domain to a regional domain, and designing an averaging scheme to transfer the data from the regional domain to the large-scale domain (Alapaty et al., 1998; Laugier et al., 1996; and the references there in). Interpolation and averaging techniques are inherently noisy, which creates numerical errors on the boundary. Often this computational noise is best described as a form of aliasing (Perkins and Smedstad, 1998). This type of aliasing is analogous to the aliasing found in data analysis caused by under sampling a continuous time series. In nesting the aliasing is caused by the difference in wave frequency between the two grids.

The Naval Coastal Model (NCOM) used to model the area of interest in this study can be configured as a passive nested or a coupled model. Currently, an increase in resolution is allowed in the horizontal but not the vertical. An interactive version of the NCOM is in development. Passive nested models use open boundary conditions to pass information from the large-scale grid to the fine mesh just as coupling does. The goal of open boundary conditions is to allow all outwardly propagating waves to leave the domain freely without causing reflections or spurious results at the boundary. Many open boundary types have been suggested, and studies (Jensen (1998), Palma and Matano (1998), and Palma and Matano(2000)) have shown that each can do a good job for certain modeling configurations. In ocean modeling the most commonly used boundary conditions are of the radiation type. These boundary conditions are based on the Sommerfeld condition, $\phi_t + c\phi_x = 0$, where ϕ is a model variable, c is the wave speed required to transmit the wave with no reflections, and the subscripts are time and space derivatives where x is the direction normal to the boundary. The major problem with this boundary condition is that the modeled and real oceans contain many waves, which travel at differing c 's. Orlanski proposed to calculate c for the dominant wave at a point just inside the boundary using a leapfrog method to approximate the Sommerfeld boundary condition. An easier to understand upstream difference form is given as (Røed and Cooper, 1986)

$$\phi_b^{n+1} = (1-r)\phi_b^n + r\phi_{b-1}^n,$$

where n is the time level, b is the boundary point, and $r = c\Delta t / \Delta x$. r is calculated numerically from

$$r = (\phi_{b-1}^n - \phi_{b-1}^{n-1}) / (\phi_{b-2}^{n-1} - \phi_{b-1}^{n-1}).$$

r 's values are confined to the limit $0 < r < 1$ for stability reasons. Unfortunately, Orlanski actually proves worse in many cases than just setting a constant c because small numerical errors corrupt the calculation (Durran, et al., 1993).

A simplification to the Orlanski boundary condition, called the Camerlengo and O'Brien radiation boundary condition is used in this study (Camerlengo and O'Brien, 1980). Camerlengo and O'Brien uses only the direction of the Orlanski boundary condition. This modifies the Orlanski relation such that if $r > 0$, then $r = 1$, and if $r < 0$, then $r = 0$. Camerlengo and O'Brien showed that this method was better than Orlanski's method for problems with Kelvin waves exiting the domain. One reason it works better is because it is a step toward a constant c solution, which deliberately overestimates the actual value of c , thus allowing more energy out of the domain.

Computational noise created by finite difference boundary conditions can be mistaken for physical results (Skamarock and Klemp, 1993 and Kurschner, 1994). This led Perkins and Smedstad (1998) to perform a frequency-decomposition to restrict conservation and continuity to the frequencies shared by the coarse and fine grids. A similar idea is employed here to reduce aliasing. In this paper, a technique based on vertical normal mode solutions at the boundary is constructed to force the fine grid with only the coarse grid information that is modally allowed on the fine mesh grid. Because radiation boundary conditions are applied to the modes and not the data values, it is easier to spot numerical noise versus physical signals in the results. The modal calculation also allows the solutions to be checked to see if the grids are physically compatible with each other.

The technique developed here is applied to a passive nesting NCOM test case of an Equatorial Kelvin wave. This technique is then applied to the same test case in two coupling situations in which the number of levels (layers) is not the same as the fine mesh; first with a NCOM coarse grid solution and secondly with a Navy Layered Ocean Model (NLOM) coarse grid solution.

2. NORMAL MODE BOUNDARY CONDITION BASICS

2.1 Model Formulation

The model used to test the normal mode open boundary conditions (NMOBC) is the Naval Coastal Ocean Model (NCOM) developed by Paul J. Martin at the Naval Research Laboratory – Stennis Space Center (Martin, 2000). This model is a hybrid sigma-z coordinate model that is designed such that the free surface is a sigma level, and the levels below the free surface are a specified number of sigma and z-levels. The model can be run with all sigma or all z-levels (except for the free surface), or any combination as long as the sigma levels overlie the z-levels. The configuration here is all sigma levels.

The model equations with the hydrostatic, Boussinesq, and incompressible approximations are given by Martin (2000) equations (1) to (8), with equation (5), the sigma equation, excluded here as

$$\frac{\partial u}{\partial t} = -\nabla \cdot (\mathbf{v}u) + Qu + fv - \frac{1}{\rho_0} \frac{\partial p}{\partial x} + F_u + \frac{\partial}{\partial z} \left(K_M \frac{\partial u}{\partial z} \right), \quad (1)$$

$$\frac{\partial v}{\partial t} = -\nabla \cdot (\mathbf{v}v) + Qv - fu - \frac{1}{\rho_0} \frac{\partial p}{\partial y} + F_v + \frac{\partial}{\partial z} \left(K_M \frac{\partial v}{\partial z} \right), \quad (2)$$

$$\frac{\partial p}{\partial z} = -\rho g, \quad (3)$$

$$\frac{\partial u}{\partial x} + \frac{\partial v}{\partial y} + \frac{\partial w}{\partial z} = Q, \quad (4)$$

$$\frac{\partial T}{\partial t} = -\nabla \cdot (\mathbf{v}T) + QT + \nabla_h (A_H \nabla_h T) + \frac{\partial}{\partial z} \left(K_H \frac{\partial T}{\partial z} \right) + Q_r \frac{\partial \gamma}{\partial z}, \quad (6)$$

$$\frac{\partial S}{\partial t} = -\nabla \cdot (\mathbf{v}S) + QS + \nabla_h (A_H \nabla_h S) + \frac{\partial}{\partial z} \left(K_H \frac{\partial S}{\partial z} \right), \quad (7)$$

$$\rho = \rho(T, S, z), \quad (8)$$

where t is the time, x , y , and z are the three coordinate directions, u , v , and w are the three components of the velocity vector, Q is a volume flux source term, \mathbf{v} is the vector velocity, T is the potential temperature, S is the salinity, ∇_h is the horizontal gradient operator, f is the Coriolis parameter, p is the pressure, ρ is the water density, ρ_0 is a reference water density, g is the acceleration of gravity, F_u and F_v are horizontal mixing terms for momentum, A_H is the horizontal mixing coefficient for scalar fields (potential temperature and salinity), K_M and K_H are vertical eddy coefficients for momentum and scalar fields, respectively, Q_r is the solar radiation, and γ is a function describing the solar extinction.

The NCOM has the capability to do one-way nesting. It currently comes coded with several different boundary conditions including Orlanski radiation boundary condition or an advective scheme for the baroclinic variables, and specified or Flather

radiation boundary condition for barotropic variables such as the surface elevation. The NMOBC developed here are applied to the baroclinic variables only.

2.2 Normal Mode Open Boundary Conditions

NMOBC for nesting a model of a single configuration is based on the work of Jensen (1998), which compares different open boundary conditions for layer ocean models. In this article vertical normal modes are used in conjunction with several different types of boundary conditions to determine whether a mode passes across an open boundary. Jensen assumes in his calculation that the stratification does not change during the model run, therefore the normal mode matrices are calculated only once at the beginning of the calculation. In the work presented here that assumption is not made, therefore the normal mode matrices are recalculated at every time step for every boundary point both for the coarse and fine meshes.

The normal modes are determined by solving for the eigenvalues and eigenvectors of the Sturm-Liouville type partial differential equation of the form

$$\left(R_z / N^2\right)_z + (gh)^{-1}R = 0 \quad (9)$$

(See Appendix A for the derivation of this form from the NCOM model equations.)

where R is only a function of z , the double z subscript denotes a second-order z derivative, N is the Brunt-Väisälä frequency, g is gravity, and h is the equivalent depth.

The eigenfunctions are found from the relation

$$AE = \lambda E, \quad (10)$$

where A is the $n \times n$ tridiagonal array formed by (9), E is the eigenvector array, and λ is the eigenvalue vector. The eigenvectors give the vertical normal modes of the model,

and the eigenvalues give the equivalent depth of each mode. Once the vertical normal modes are known the related modal component of a model variable is determined by (Jensen, 1993)

$$\tilde{U}_k = \sum_{j=1}^N (\alpha_{jk})^{-1} U_j, \quad (11)$$

where U_j is a model variable at a level j and can be a velocity component or a scalar such as potential temperature or salinity, $(\alpha_{jk})^{-1}$ is the inverse of the eigenvector matrix, and \tilde{U}_k is the related modal component for mode k . Once \tilde{U} is determined for each mode, a radiation boundary condition is applied to it. For the purpose of this study, the simple Camerlengo and O'Brien (1980) radiation boundary condition is sufficient, but more complex boundary conditions may also be used. After the radiation boundary condition is applied (11) is inverted to reconstruct the model variable.

Because the Camerlengo and O'Brien radiation boundary condition is a simplification of the Orlanski method, much of the existing NCOM Orlanski model code was used in the implementation of the NMOBC. In the NCOM, the Orlanski radiation condition uses a leapfrog temporal scheme and is formulated as (Rochford and Martin, 2001)

$$V_t(B, N+1) = \frac{1}{1+a} [(1-a)V_t(B, N-1) + 2aV_t(B-1, N)], \quad (13)$$

where V_t is either a velocity or scalar at a given boundary point t , B denotes the grid point location of the boundary, $B-1$ denotes the first interior grid point location from the boundary, N denotes the time level, and a is given by

$$a = \max[0, \min[1, c\Delta t / \Delta x]] \quad (14)$$

where

$$\frac{c\Delta t}{\Delta x} = \frac{V_i(B-1, N-1) - V_i(B-1, N+1)}{V_i(B-1, N+1) + V_i(B-1, N-1) - 2V_i(B-2, N)}. \quad (15)$$

This requires values of V_i at the three time levels $N-1$, N , and $N+1$.

The NMOBC, using the Camerlengo and O'Brien radiation condition, calculation is completed similarly to the Orlanski calculation, but instead of V_i being a baroclinic velocity or scalar it is the corresponding modal velocity or scalar. Also, a is calculated but it is assigned such that if $a < 0$, $a = 0$ and if $a > 0$, $a = 1$. This acts as a direction, such that $a = 0$ is flow out of the domain and $a = 1$ is flow into the domain, and reduces equation (13) to

$$V_i(B, N+1) = (1-a)V_i(B, N-1) + aV_i(B-1, N) \quad (16)$$

This calculation is performed on both the fine mesh and the coarse mesh. The incoming and outgoing signals are then combined in the following manner. If the direction calculation of both grids suggest that the wave signal is into the fine mesh interior then the coarse mesh solution is used. If the direction calculation of both grids suggest that the wave signal is out of the fine mesh then the fine mesh solution is used. If the direction calculation of the two grids disagree then the average of the two solutions is used. The determination of signal propagation direction is performed for each mode separately. Once the new modal solutions are formed using the Camerlengo and O'Brien radiation boundary condition, they are summed using the inverse of (11) to find the updated baroclinic velocity or scalar at a point along the boundary.

2.3 Numerical Example

A numerical example is offered to clarify the NMOBC's procedure. In this example, the calculations will be performed for an actual scalar boundary point of the

first numerical test case that is discussed in the following section. For this test case there are 14 sigma levels that are uniformly distributed in the vertical. There are 13 scalar sigma levels at the midpoints of the main z-grid levels. Potential temperature is initialized to 20.0 °C for all 13 vertical levels, and salinity is initialized as a linear distribution from 35.0 ppt at the surface to 40.2 ppt at the bottom. The salinity distribution approximately gives the desired stability value of $N = 8.8 \times 10^{-3} \text{ s}^{-1}$. To keep the coarse and fine mesh values from being identical, the example calculations will be given after a one-day integration period.

The first step is to calculate the density distribution from the temperature and salinity profiles. The method used for the NMOBC density calculation is proposed in Brydon et al. (1999) and is used because they claim that this method is as accurate as Mellor's (1991) UNESCO calculation but is more computationally efficient. This method calculates density from a seven-term polynomial cubic in potential temperature and linear in salinity such that

$$\sigma(T, S, p) = C_1(p) + C_2(p)T + C_3(p)S + C_4(p)T^2 + C_5(p)ST + C_6(p)T^3 + C_7(p)ST^2, \quad (17)$$

where $\sigma = \rho - 1000 \text{ kg m}^{-3}$. The coefficients, $C_n(p)$, are calculated through a two-stage least square fitting procedure and are of the form $C_n(p) = \alpha_n + \beta_n p + \gamma_n p^2$ where p is the pressure. To calculate the Brünt-Väisälä frequency the pressure differences are ignored, i.e. $p=0$. The density calculation results for the test case are in Table 1.

Next, the square Brünt-Väisälä frequencies are calculated for the 14 sigma-levels. This is done by calculating $N^2 = -g\rho_0^{-1}\sigma_z$ using center differences for the interior 12 levels and then linearly interpolating to the ends. See Figure 1 for the N^2 finite difference

Table 1: Density calculation input and results rounded to the nearest thousandths. CM is the coarse mesh calculation. FM is the fine mesh calculation. T is the potential temperature. S is the salinity. σ is the density.

Level	CM-T (°C)	CM-S (ppt)	CM- σ (kg m ⁻³)	FM-T (°C)	FM-S (ppt)	FM- σ (kg m ⁻³)
1	20.00000	35.19968	24.93680	20.000	35.19973	24.93684
2	19.99995	35.59764	25.23873	20.000	35.59771	25.23877
3	19.99995	35.99606	25.54100	20.000	35.99610	25.54102
4	19.99995	36.39454	25.84332	20.000	36.39460	25.84335
5	19.99997	36.79295	26.14557	20.000	36.79297	26.14558
6	19.99997	37.19141	26.44787	20.000	37.19155	26.44797
7	19.99997	37.58988	26.75018	20.000	37.58987	26.75017
8	19.99997	37.98836	27.05249	20.000	37.98838	27.05250
9	19.99997	38.38677	27.35475	20.000	38.38675	27.35473
10	19.99997	38.78524	27.65706	20.000	38.78523	27.65705
11	19.99997	39.18366	27.95933	20.000	39.18366	27.95932
12	19.99997	39.58210	28.26161	20.000	39.58211	28.26162
13	20.00000	39.98006	28.56353	20.000	39.98018	28.56362

locations. Use the density values from Table 1 and ρ_0 , which has a model assigned value of 1025 kg m⁻³, to give the N^2 values recorded in Table 2.

The calculation of the eigenvalues and eigenvectors at the 13 scalar sigma levels are next. First equation (35A) is put in its finite difference form with $R=p(z)$ and $\lambda=(gh)^{-1}$.

$$\frac{1}{z_{k+1} - z_k} \left[\frac{1}{N_{k+1}^2} \left(\frac{p_{q+1} - p_q}{z_{q+1} - z_q} \right) - \frac{1}{N_k^2} \left(\frac{p_q - p_{q-1}}{z_q - z_{q-1}} \right) \right] + \lambda p_q = 0, \quad (18)$$

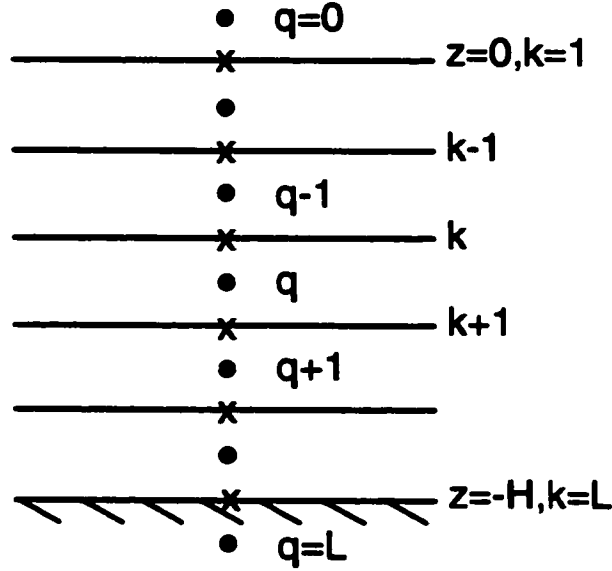


Figure 1: z-grid showing positions of N^2 and p . p is given at the locations marked with a dot, and N^2 is located at points marked with and x.

where the relative positions of N^2 and p are given in Figure 1. Rewrite equation (18) as

$$\begin{aligned}
 & p_q \left[\frac{-1}{N_{k+1}^2 (z_{k+1} - z_k)(z_{q+1} - z_q)} - \frac{1}{N_k^2 (z_{k+1} - z_k)(z_q - z_{q-1})} + \lambda \right] \\
 & + p_{q+1} \left[\frac{1}{N_{k+1}^2 (z_{k+1} - z_k)(z_{q+1} - z_q)} \right] + p_{q-1} \left[\frac{1}{N_k^2 (z_{k+1} - z_k)(z_q - z_{q-1})} \right] = 0,
 \end{aligned} \tag{19}$$

where the coefficients of p_q will be placed on the diagonals of a tridiagonal matrix, and the coefficients of p_{q-1} are the subdiagonals and the coefficients of p_{q+1} are the superdiagonals of the matrix. Note that the tridiagonal matrix is symmetric about the diagonal. To solve for the coefficients of (19) boundary conditions need to be applied. The boundary conditions applied here are those of Gill (1982) where $R = \hat{p}$.

$$\frac{d\hat{p}}{dz} + \frac{N^2}{g} \hat{p} = 0 \quad \text{at } z=0. \tag{20}$$

and

$$\frac{d\hat{p}}{dz} = 0 \quad \text{at } z=-H \quad (21)$$

Table 2: Square Brünt-Väisälä frequencies (N^2) calculated by the model. CM is the coarse mesh values. FM is the fine mesh values.

levels	CM - N^2 (s^{-1})	FM- N^2 (s^{-1})
1	7.49743×10^{-5}	7.49823×10^{-5}
2	7.50572×10^{-5}	7.50582×10^{-5}
3	7.51402×10^{-5}	7.51340×10^{-5}
4	7.51506×10^{-5}	7.51549×10^{-5}
5	7.51364×10^{-5}	7.51316×10^{-5}
6	7.51463×10^{-5}	7.51644×10^{-5}
7	7.51502×10^{-5}	7.51255×10^{-5}
8	7.51501×10^{-5}	7.51549×10^{-5}
9	7.51383×10^{-5}	7.51326×10^{-5}
10	7.51487×10^{-5}	7.51516×10^{-5}
11	7.51407×10^{-5}	7.51397×10^{-5}
12	7.51431×10^{-5}	7.51464×10^{-5}
13	7.50510×10^{-5}	7.50719×10^{-5}
14	7.49590×10^{-5}	7.49974×10^{-5}

Using the N^2 's in Table 2, the diagonals and subdiagonals are calculated and placed in Table 3. This tridiagonal matrix is then solved using the LAPACK eigenvalue-eigenvector solver SSTEVM. The eigenvalues are the λ 's of equation (19) and the eigenvectors are the normal mode solutions. The eigenvalues, λ^{-1} , are equal to the square

Table 3: Calculated values of the coefficients from equation (19) where the diagonals are the coefficients for p_q and the subdiagonals are the coefficients for p_{q-1} .

Levels	CM diagonal	CM subdiagonal	FM diagonal	FM subdiagonal
1	9.01179	-----	9.01167	-----
2	18.00301	-9.00648	18.00364	-9.00637
3	17.99182	-8.99653	17.99202	-8.99727
4	17.99227	-8.99529	17.99233	-8.99478
5	17.99278	-8.99699	17.99119	-8.99755
6	17.99114	-8.99580	17.99194	-8.99364
7	17.99069	-8.99534	17.99307	-8.99830
8	17.99210	-8.99534	17.99221	-8.99477
9	17.99227	-8.99676	17.99261	-8.99744
10	17.99199	-8.99551	17.99176	-8.99517
11	17.99268	-8.99648	17.99239	-8.99660
12	18.00341	-8.99619	18.00051	-8.99579
13	9.00722	-9.00722	9.00471	-9.00471

of the phase speed, c , and also equal to gh , so the dynamic height of each mode is known.

Table 4 gives the eigenvalues and the phase speeds of Table 3's tridiagonal matrix and

Table 5 gives the barotropic and first three baroclinic normal modes.

Notice that the baroclinic modes are sine waves with the number of zero crossings equal to the mode number. This pattern continues for modes not included in Table 5.

There is now only one step left before applying equation (11) and changing to modal space. That step is to invert the eigenvector matrix. This is accomplished by applying the LAPACK subroutines SGETRF and SGETRI. SGETRF preconditions the matrix by

Table 4: Calculated eigenvectors and their corresponding phase speeds. Recall mode number 0 corresponds to the barotropic mode, and mode numbers 1 – 12 are the baroclinic modes.

Mode number	CM λ (s/m) ²	CM c (m/s)	FM λ (s/m) ²	FM c (m/s)
0	4.07695x10 ⁻⁴	49.52585	4.06742x10 ⁻⁴	49.58387
1	0.52363	1.38194	0.52363	1.38193
2	2.06184	0.69642	2.06180	0.69643
3	4.52621	0.47004	4.52626	0.47003
4	7.77412	0.35865	7.77380	0.35866
5	11.61624	0.29340	11.61615	0.29341
6	15.82947	0.25134	15.82871	0.25135
7	20.16833	0.22267	20.16736	0.22268
8	24.38018	0.20253	24.37998	0.20253
9	28.22042	0.18824	28.21929	0.18825
10	31.46421	0.17828	31.46458	0.17827
11	33.92640	0.17168	33.92579	0.17169
12	35.46170	0.16793	35.46228	0.16793

performing a Lower-Upper factorization. SGETRI calculates the inverse of the output from SGETRF. Note that the inverse of the eigenvector matrix is approximately equal to the transpose of the matrix.

Next, the modal components are calculated using equation (11) and the results for salinity are shown in Table 6. Note: for temperature and salinity a mean value must be removed from U_j before (11) is applied to reduce numerical error in the calculation.

Table 5: The barotropic (mode=0) and first three baroclinic normal modes. CM is the coarse mesh and FM is the fine mesh.

level	CM mode=0	CM mode=1	CM mode=2	CM mode=3	FM mode=0	FM mode=1	FM mode=2	FM mode=3
1	0.27672	0.38931	0.38084	0.36671	0.27672	0.38931	0.38082	0.36670
2	0.27687	0.36690	0.29388	0.18264	0.27687	0.36691	0.29387	0.18263
3	0.27701	0.32312	0.13947	-0.09352	0.27701	0.32312	0.13948	-0.09351
4	0.27714	0.26052	-0.04693	-0.32267	0.27714	0.26052	-0.04692	-0.32267
5	0.27725	0.18277	-0.22253	-0.38944	0.27725	0.18277	-0.22251	-0.38944
6	0.27735	0.09437	-0.34716	-0.26027	0.27735	0.09435	-0.34717	-0.26024
7	0.27744	0.00047	-0.39222	-0.00014	0.27744	0.00049	-0.39222	-0.00021
8	0.27751	-0.09345	-0.34738	0.26006	0.27751	-0.09345	-0.34737	0.26003
9	0.27758	-0.18192	-0.22293	0.38939	0.27758	-0.18191	-0.22294	0.38938
10	0.27763	-0.25982	-0.04737	0.32280	0.27763	-0.25981	-0.04738	0.32283
11	0.27766	-0.32258	0.13903	0.09392	0.27766	-0.32258	0.13902	0.09387
12	0.27769	-0.36657	0.29357	-0.18237	0.27769	-0.36657	0.29356	-0.18234
13	0.27770	-0.38919	0.38072	-0.36659	0.27770	-0.38920	0.38074	-0.36662

Table 6: Modal components of salinity upon application of equation (11) where the mean salinity value has been subtracted. CM is the coarse mesh results. FM is the fine mesh results.

Mode	CM – modal salinity	FM – modal salinity
1	9.34383	9.34397
2	-5.32836	-5.32833
3	-7.74860×10^{-6}	6.06775×10^{-5}
4	0.58062	-0.58066
5	2.28882×10^{-5}	3.45707×10^{-7}
6	-0.19912	-0.19914
7	-1.19209×10^{-5}	-7.09295×10^{-5}
8	-9.24672×10^{-2}	-9.24729×10^{-2}
9	1.26362×10^{-5}	-8.70228×10^{-6}
10	4.63802×10^{-2}	-4.63663×10^{-2}
11	8.76188×10^{-6}	6.02007×10^{-6}
12	-1.98931×10^{-2}	-1.98981×10^{-2}
13	3.57628×10^{-6}	-1.80304×10^{-5}

Next $c \Delta t / \Delta x$ is calculated using equation (15) and a propagation direction, α , is found. The propagation direction is given in Table 7 for each mode. Note that the values calculated from (15) represent inflow or outflow of the grid it is calculated on.

Therefore, the coarse mesh values must be switched to reflect inflow or outflow on the associated fine mesh, for example, if the coarse mesh value from (15) equals 1.0 it is changed to equal 0.0. Next the radiation condition (16) is applied to the modal salinities for the coarse and fine meshes. The coarse and fine mesh modal components are

combined to form a single new modal component. Here the combining is done by using the coarse mesh value if the direction of both meshes is into

Table 7: The direction of propagation calculated from the sign of the results of equation (15). Direction equal to 0.0 results in propagation into the fine mesh. Direction equal to 1.0 results in propagation out of the fine mesh. CM is the coarse mesh results. FM is the fine mesh results.

Mode	CM - direction	FM – direction
1	0.0	1.0
2	1.0	1.0
3	1.0	0.0
4	1.0	0.0
5	1.0	0.0
6	0.0	1.0
7	0.0	1.0
8	0.0	1.0
9	0.0	1.0
10	1.0	1.0
11	1.0	0.0
12	1.0	0.0

the fine mesh, the fine mesh value if the direction of both meshes is out of the fine mesh, and average the fine and coarse mesh values if the directions oppose each other. This gives the new modal component given in Table 8.

Next the inverse of equation (11) is applied to revert from modal space to model space. This gives the new boundary values for salinity, shown in Table 8, after the mean value has been re-added.

Table 8: Modal Salinity after the radiation condition has been applied and the combining of the fine and the coarse mesh solutions is completed. Final Salinity is the result of applying the inverse of equation (11) and adding back the mean salinity value.

Mode	Modal Salinity	Final Salinity
1	9.34397	35.19970
2	-5.32836	35.59767
3	-4.51891×10^{-5}	35.99606
4	-0.58063	36.39459
5	3.57054×10^{-5}	36.79299
6	-0.19913	37.19157
7	-5.01253×10^{-5}	37.58992
8	-9.24796×10^{-2}	37.98841
9	-3.49681×10^{-6}	38.38680
10	-4.63756×10^{-2}	38.78525
11	8.53450×10^{-6}	39.18366
12	-1.99141×10^{-2}	39.58207
13	5.38815×10^{-6}	39.98016

3. NUMERICAL TESTS

3.1 Gaussian Perturbation – Nested NCOM

An Equatorial Kelvin wave propagation study is used as a numerical test for the NMOBC. In particular, a gaussian perturbation symmetric about the equator is added to salinity and then allowed to evolve in an ocean initially at rest. The perturbation is determined by

$$s_1 = S + \delta s \exp\left[\frac{-(x^2 + y^2)}{L^2}\right] \quad (22)$$

where $x = (\lambda - \lambda_0)\cos\phi$, $y = (\phi - \phi_0)$, λ_0 and ϕ_0 are the values of longitude and latitude at the center of the perturbation, respectively. For this study, λ_0 is equal to 164.390625°W, and ϕ_0 is equal to 0.0°N. L is 500 km, S is the original value of salinity, which is a linear transform with 35.0 ppt at the surface and 40.2 ppt at the bottom, which gives a constant N_2 profile, and δs is the first baroclinic mode salinity perturbation. See Appendix C for the calculation used in this study. Similar tests have been conducted using layer models of the ocean (Ginis et al., 1998) and ocean-atmosphere coupling (Philander et al. 1984).

The NCOM for this test case is run with a 1:2 nesting ratio. The large domain of the study is 109.125°E to 70.875°W and 21.0°N to 21.0°S with a grid of 248x81 and $\Delta x = 0.703125^\circ$ and $\Delta y = 0.5^\circ$. The nest domain of the study is 151.559°W to 130.816°W and 9.875°N to 9.875°S with a grid of 60x80 and $\Delta x = 0.3515625^\circ$ and $\Delta y = 0.25^\circ$. The large

domain contains the Pacific Ocean coastline, but the bathymetry for it and the small domain is set to a flat bottom of 500 m to simplify the modal calculations for the test case, islands; however, are retained. The northern and southern boundaries of the large domain are closed. Both models are run with 14 sigma levels evenly spaced in the vertical. The perturbation is centered in the large domain. The time increment is 30 minutes for the coarse mesh and 15 minutes for the fine mesh.

Because the ultimate goal of this research is to link unlike physics, the goal of this test is to have model results as good as using the boundary condition options included with the NCOM, e.g. Orlanski radiation boundary conditions for scalars and normal baroclinic velocities and a zero gradient condition for tangential baroclinic velocities.

Figures 2 and 3 illustrate the salinity field and currents of this test case where the axisymmetric perturbation propagates as a Rossby wave to the west and as a Kelvin wave to the east. The salinity and currents show a smooth transition in the fine mesh region from the constant density per level with no flow state to the perturbed state. When the Kelvin wave perturbation leaves the fine mesh region there is minimal reflection as the wave initially impacts the open boundary. Especially notice that the salinity reflections in these plots are on the order of 2×10^{-3} ; therefore in most modeling cases these reflections would not even be noticeable. The NMOBC gives similar results as compared to the Orlanski and zero gradient solution and can be considered a successful nesting boundary condition.

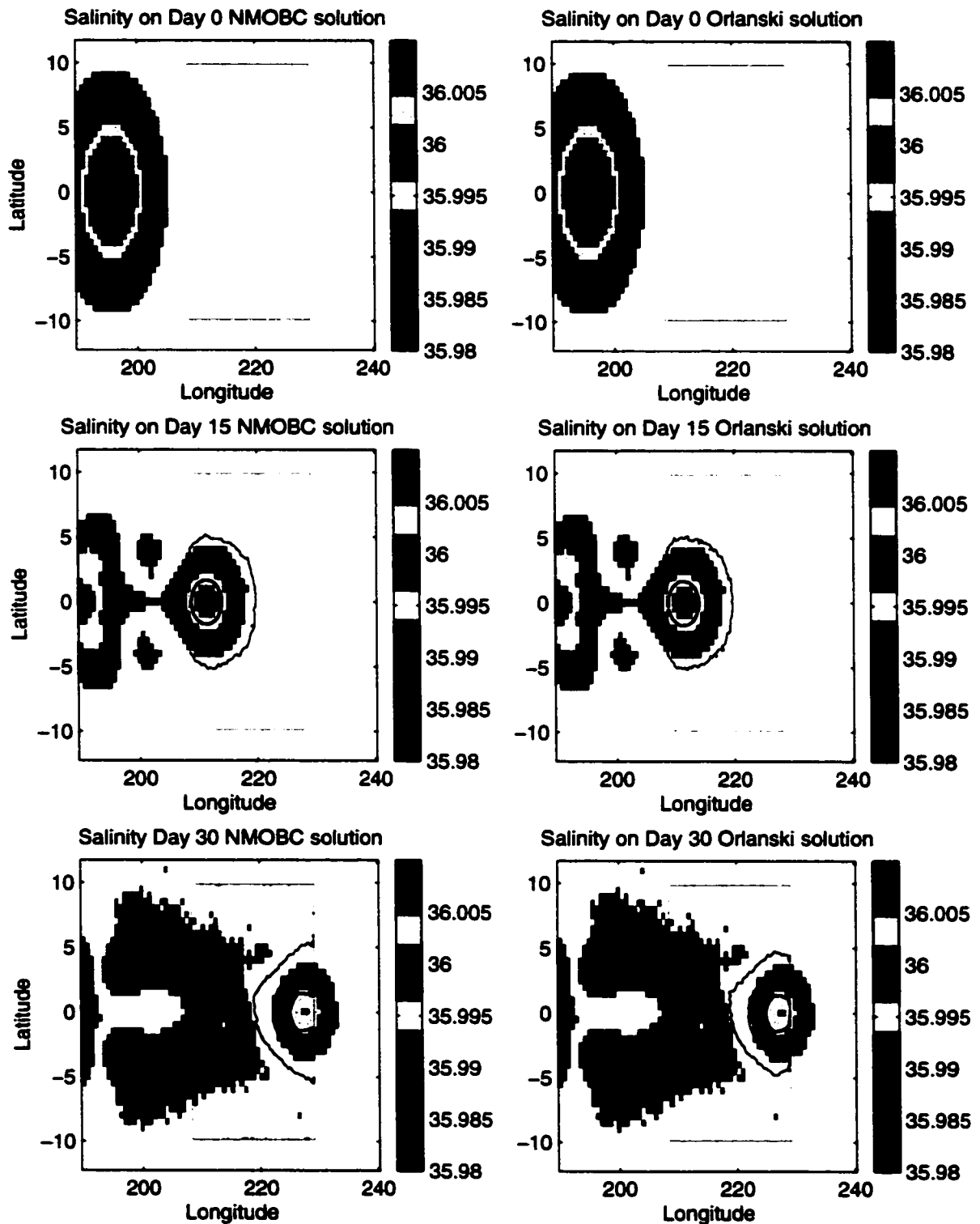


Figure 2: Salinity results of the CM NCOM for days 0, 15, and 30, with contours of the NMOBC salinity result in the left column and contours of the Orlanski results in the right column. FM bounding box is in gray. Contours match the color-scale interface values.

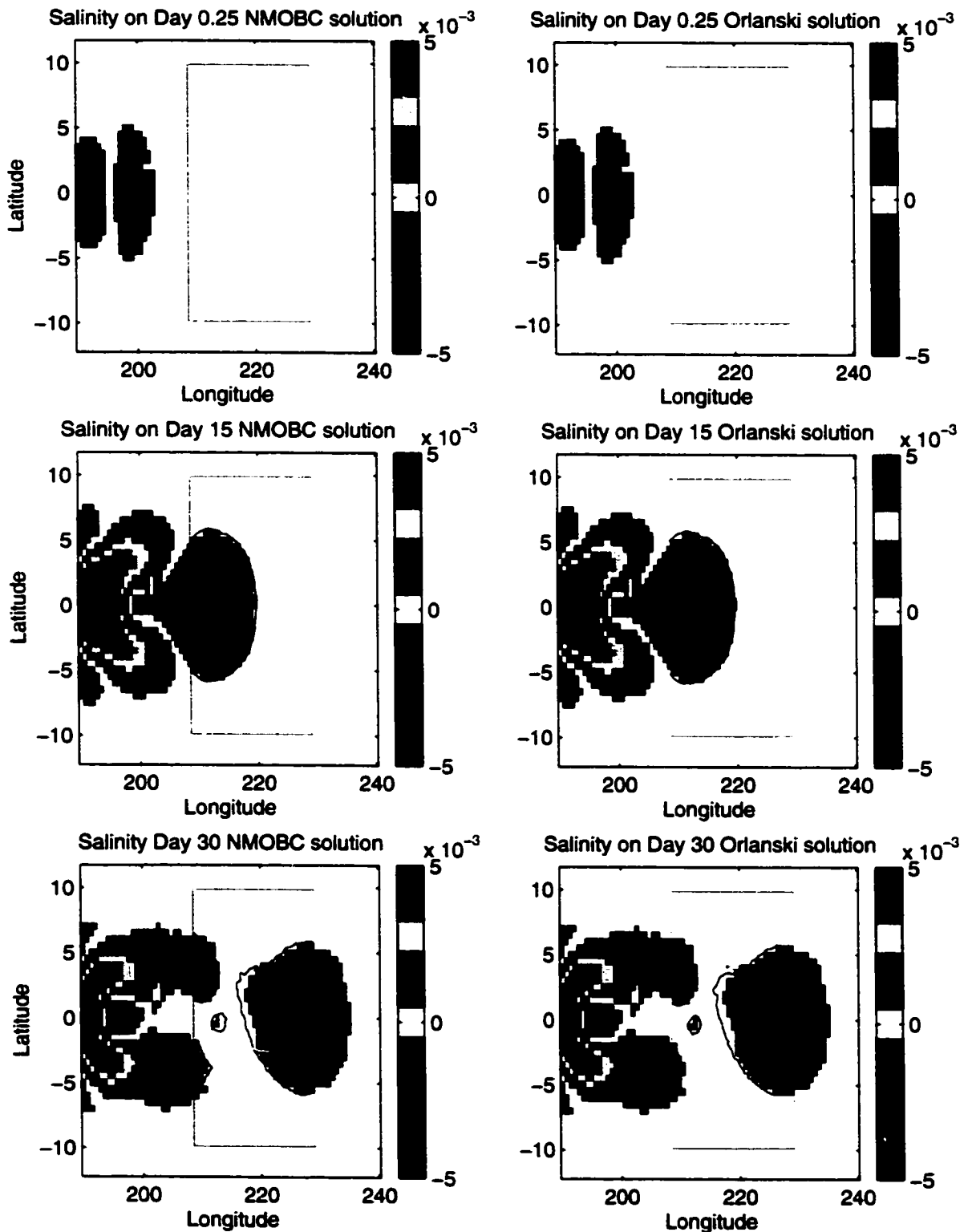


Figure 3: U-Velocity results of the CM NCOM for days 0.25, 15, and 30, with contours of the NMOBC salinity result in the left column and contours of the Orlandi results in the right column. FM bounding box is in gray. Contours match the color-scale interface values.

3.2 Gaussian Perturbation – Coupled NCOM

In this test case, the coarse mesh model is the same as in the test case presented in section 3.1 except that instead of 14 sigma levels the model now only has 6 sigma levels with a time step of 20 minutes. This reduction in sigma levels is comparable to the operational NLOM set up of 6 layers. The fine mesh is also the same except now there are 40 sigma levels with a time step of 800 seconds. The number of sigma levels is chosen to be approximately the value commonly used in coastal simulations. The NCOM does not currently allow differences in the number sigma levels between the coarse and fine mesh in a nested simulation so the model is run in a coupled situation. The coarse mesh is run with the Gaussian perturbation first, saving output every six hours. This output is then used as input to the fine mesh model with the data interpolated to each fine mesh time step inside the NCOM model run. The coarse mesh simulation is also run at the fine mesh horizontal resolution with 40 sigma levels and a time step of 400 seconds for comparison purposes.

Two runs are completed for the fine mesh. First, an Orlanski radiation boundary condition case is run where the input data is interpolated from the coarse mesh grid to the fine mesh horizontal and vertical grid structure. In the portion of the vertical grid where no information on the coarse mesh is known, i.e. near the surface and near the bottom, filling of the nearest value is performed. Second, a NMOBC case is run where the input data is interpolated in the horizontal but not in the vertical. Because there is a difference in the number of eigenvectors in six-level coarse mesh and the 40-level fine mesh there is no longer a one-to-one ratio for radiation boundary conditions to applied to each mode. In this case, the NMOBC's are applied to the first six modes where both models have

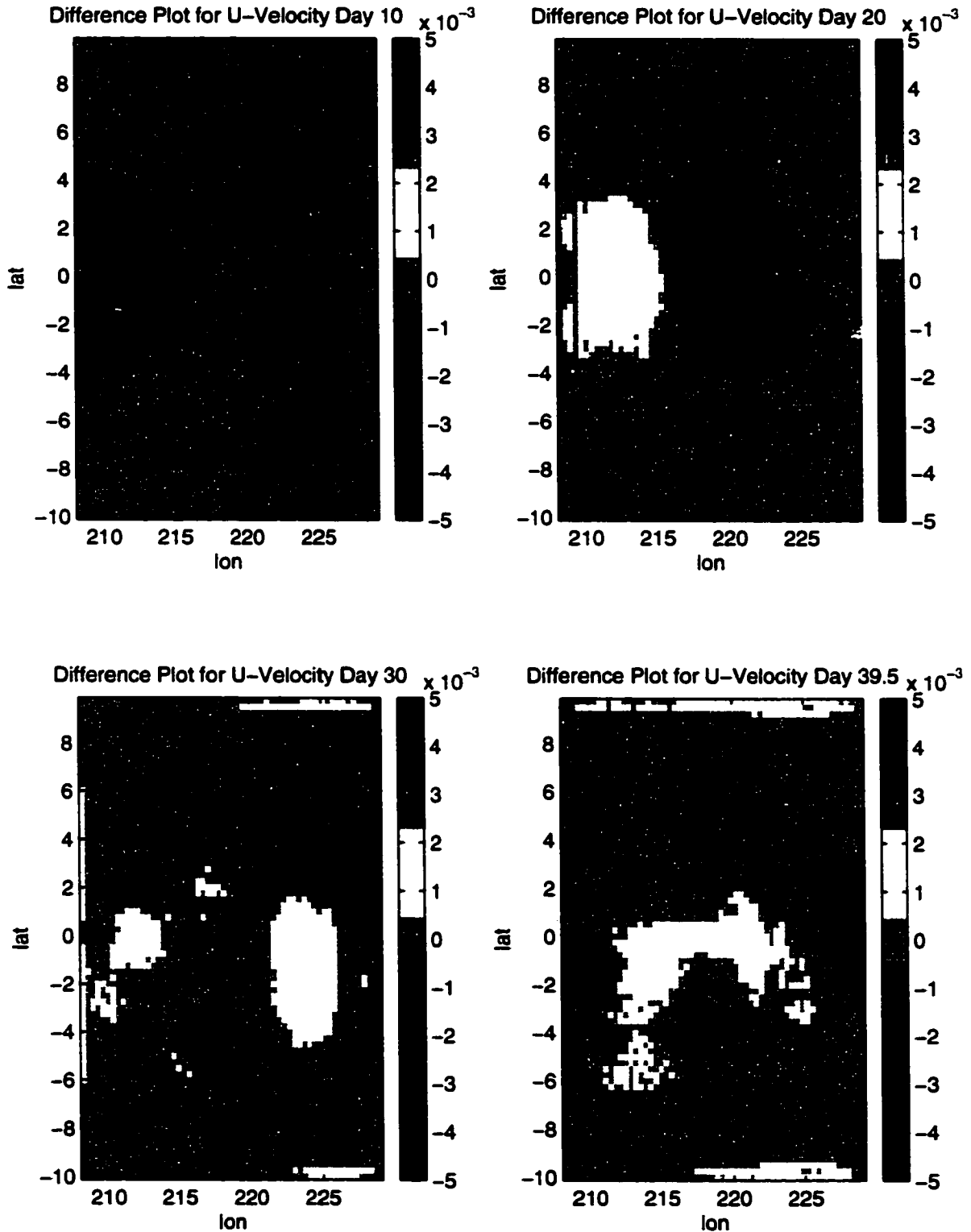


Figure 4: Difference plot for level 3 U-Velocity of the coarse mesh NCOM run at the fine mesh resolution and the NMOBC solution for the coupled NCOM to NCOM fine mesh at days 10, 20, 30, and 40.

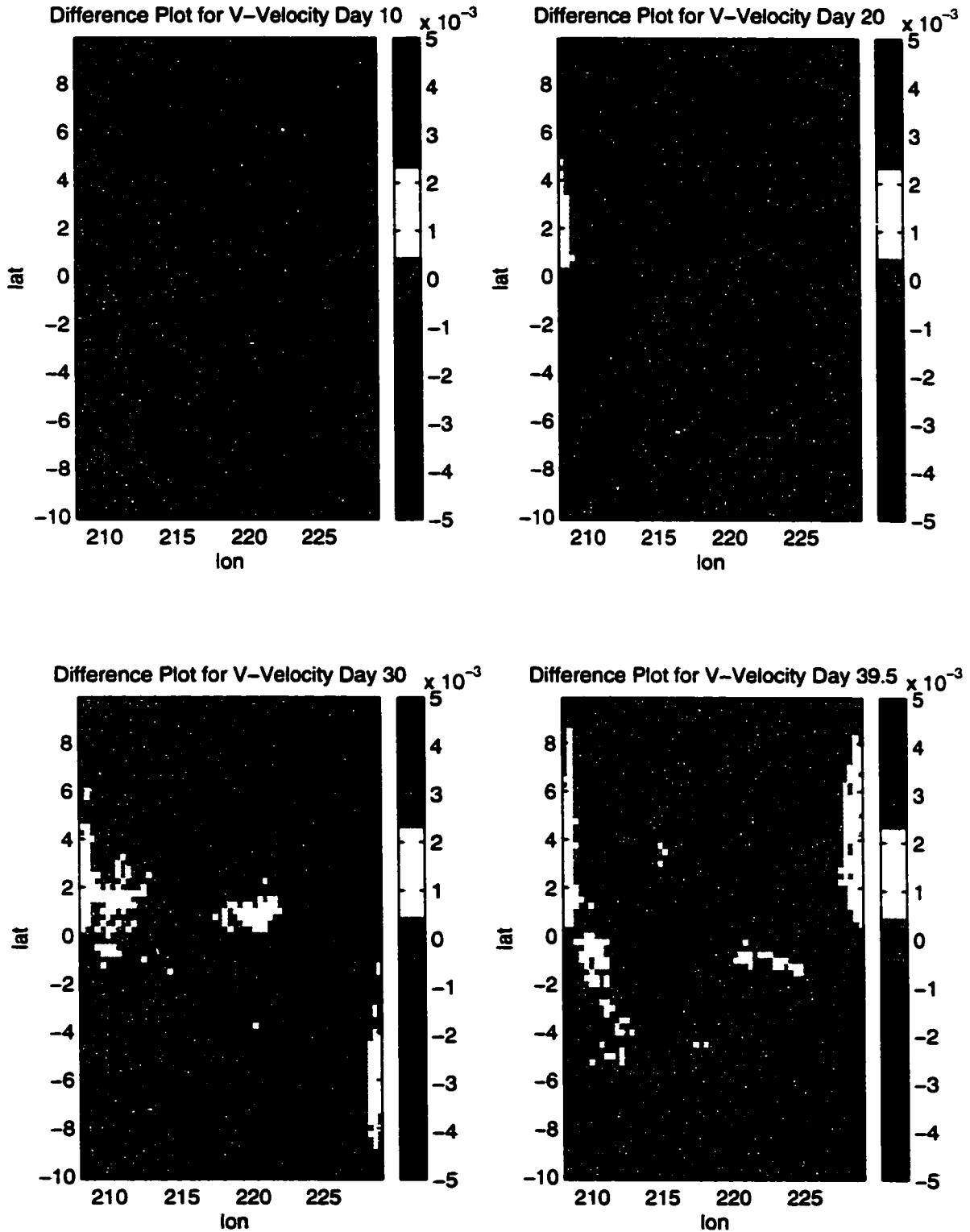


Figure 5: Difference plot for level 3 V-Velocity of the coarse mesh NCOM run at the fine mesh resolution and the NMOBC solution for the coupled NCOM to NCOM fine mesh at days 10, 20, 30, and 40.

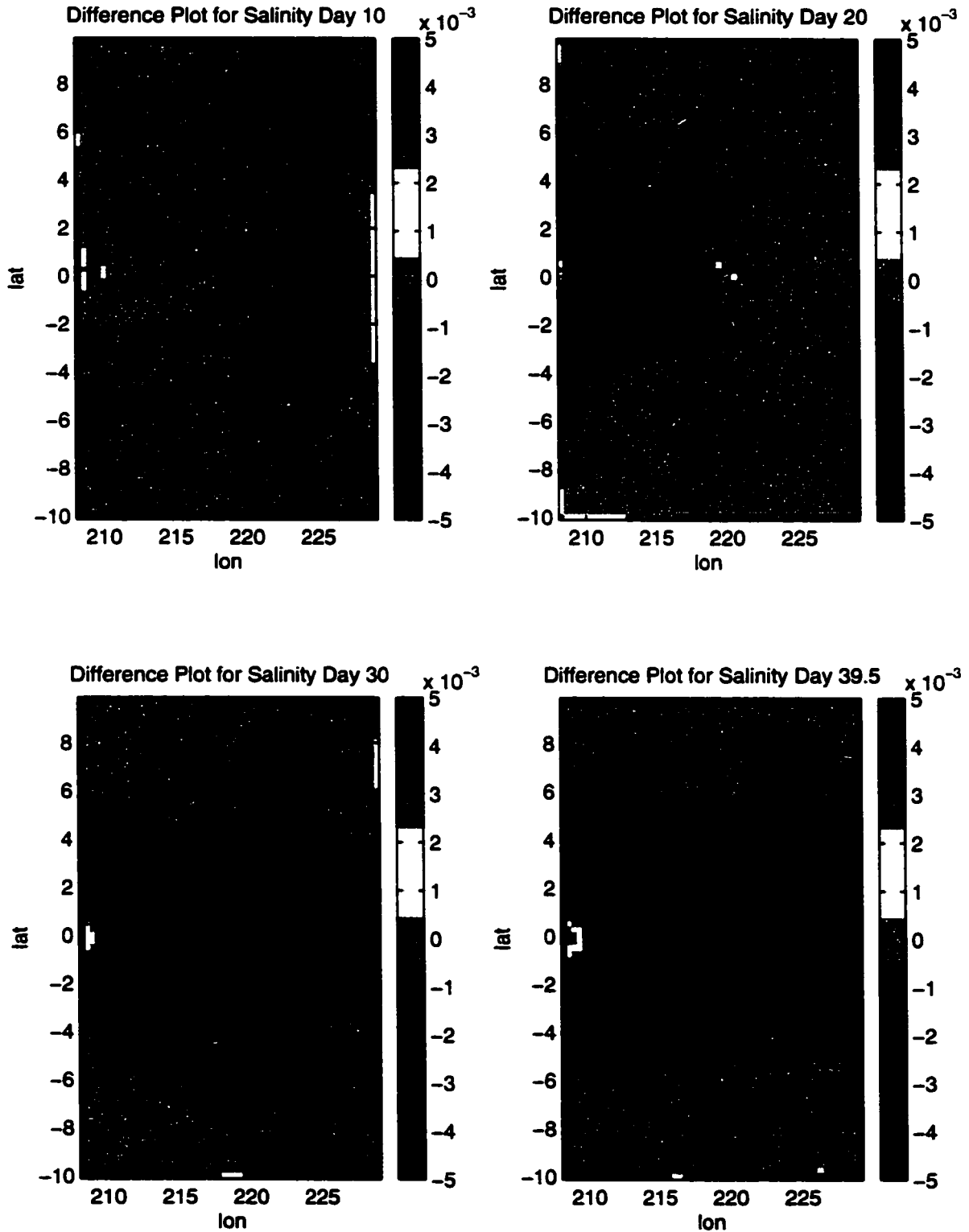


Figure 6: Difference plot for level 3 Salinity of the coarse mesh NCOM run at the fine mesh resolution and the NMOBC solution for the coupled NCOM to NCOM fine mesh at days 10, 20, 30, and 40.

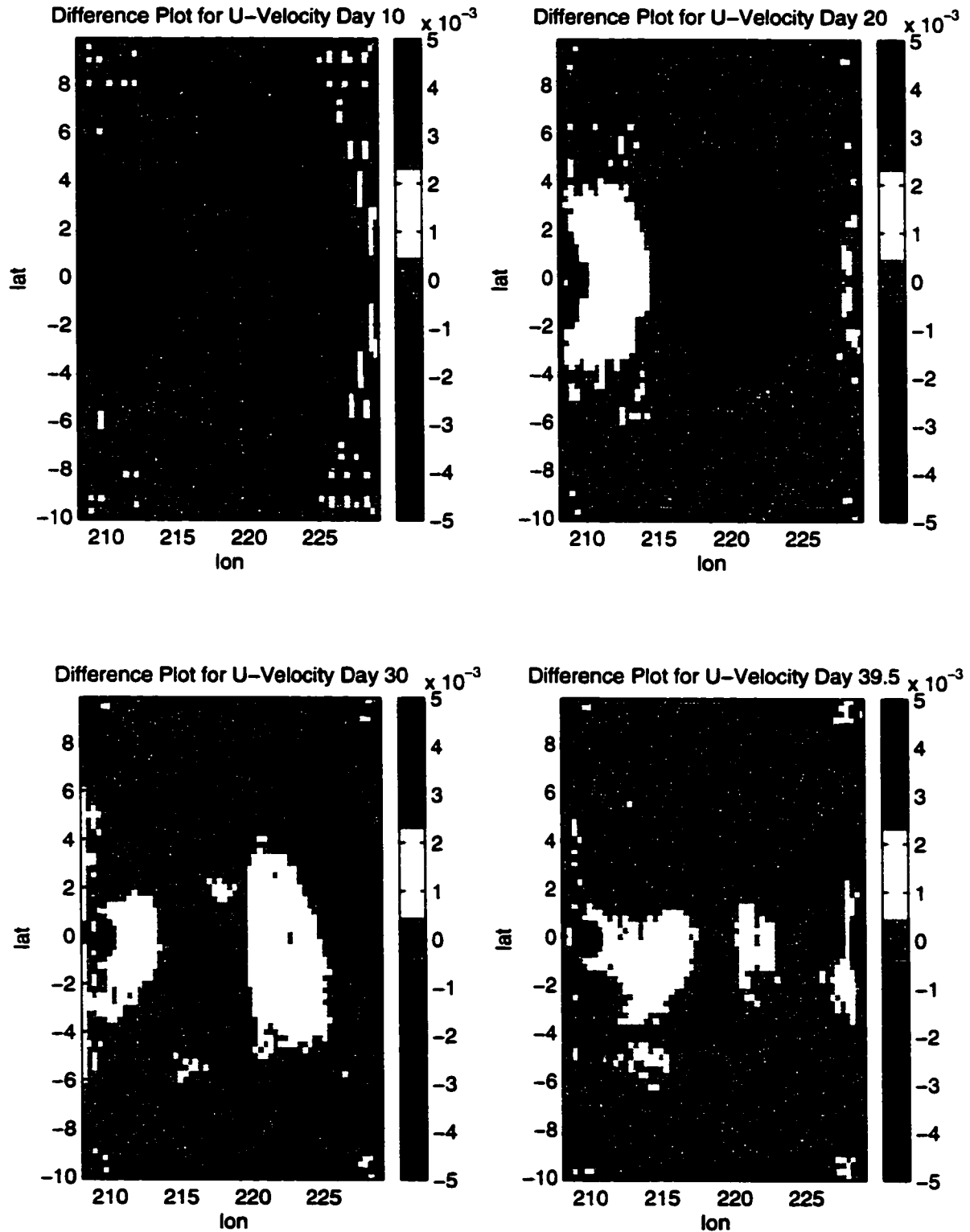


Figure 7: Difference plot for level 3 U-Velocity of the coarse mesh NCOM run at the fine mesh resolution and the Orlandi solution for the coupled NCOM to NCOM fine mesh at days 10, 20, 30, and 40.

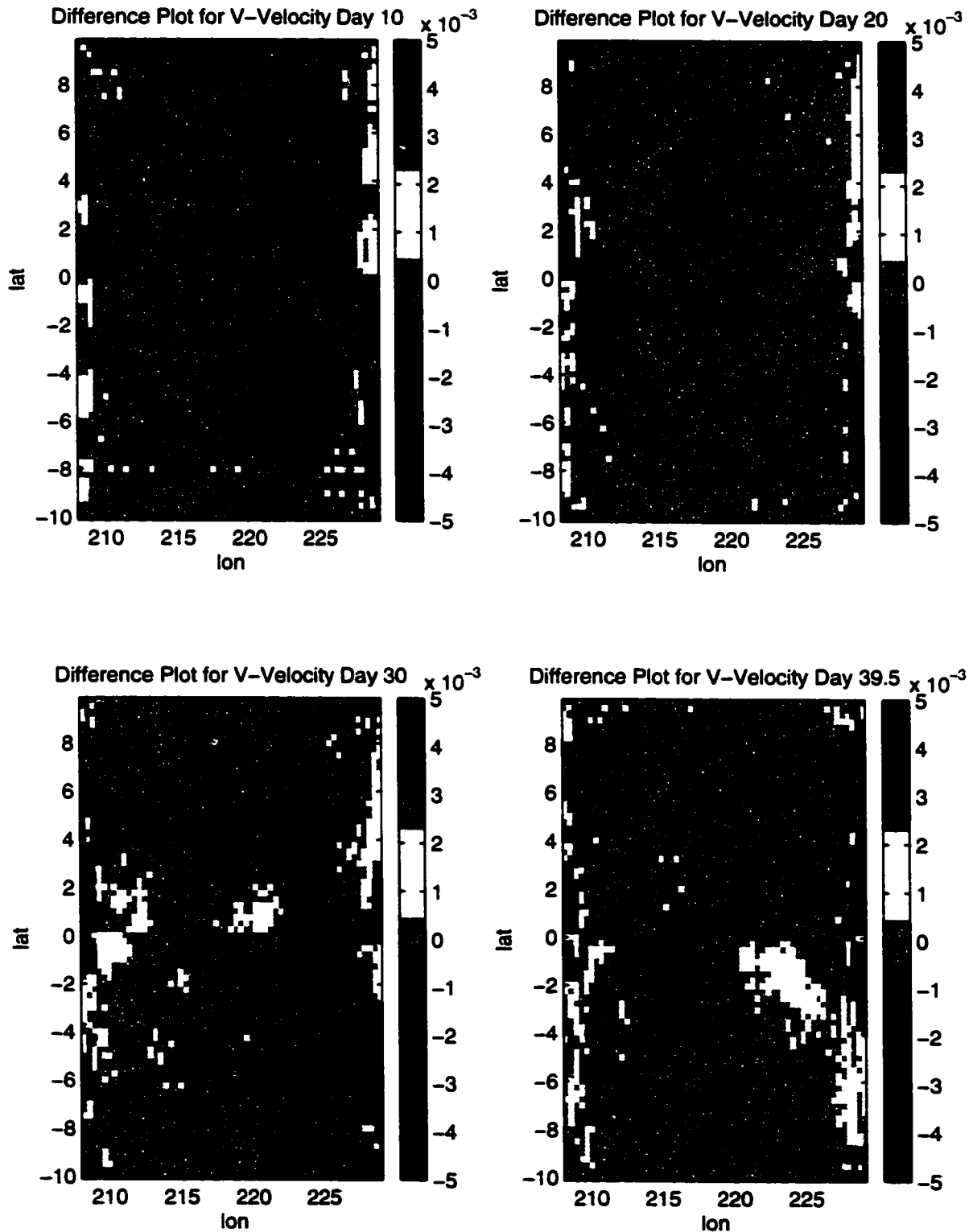


Figure 8: Difference plot for level 3 V-Velocity of the coarse mesh NCOM run at the fine mesh resolution and the Orlanski solution for the coupled NCOM to NCOM fine mesh at days 10, 20, 30, and 40.

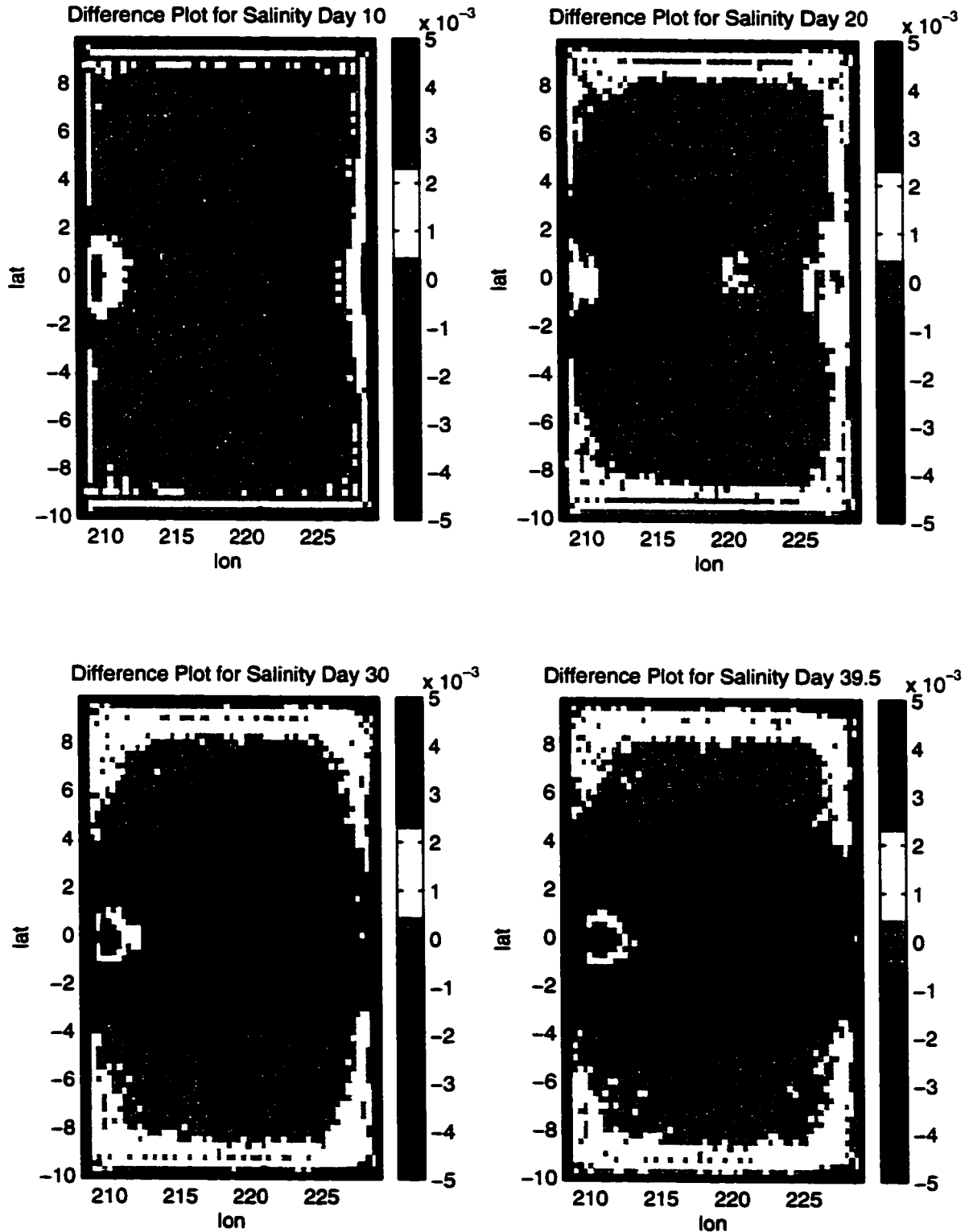


Figure 9: Difference plot for level 3 Salinity of the coarse mesh NCOM run at the fine mesh resolution and the Orlandi solution for the coupled NCOM to NCOM fine mesh at days 10, 20, 30, and 40.

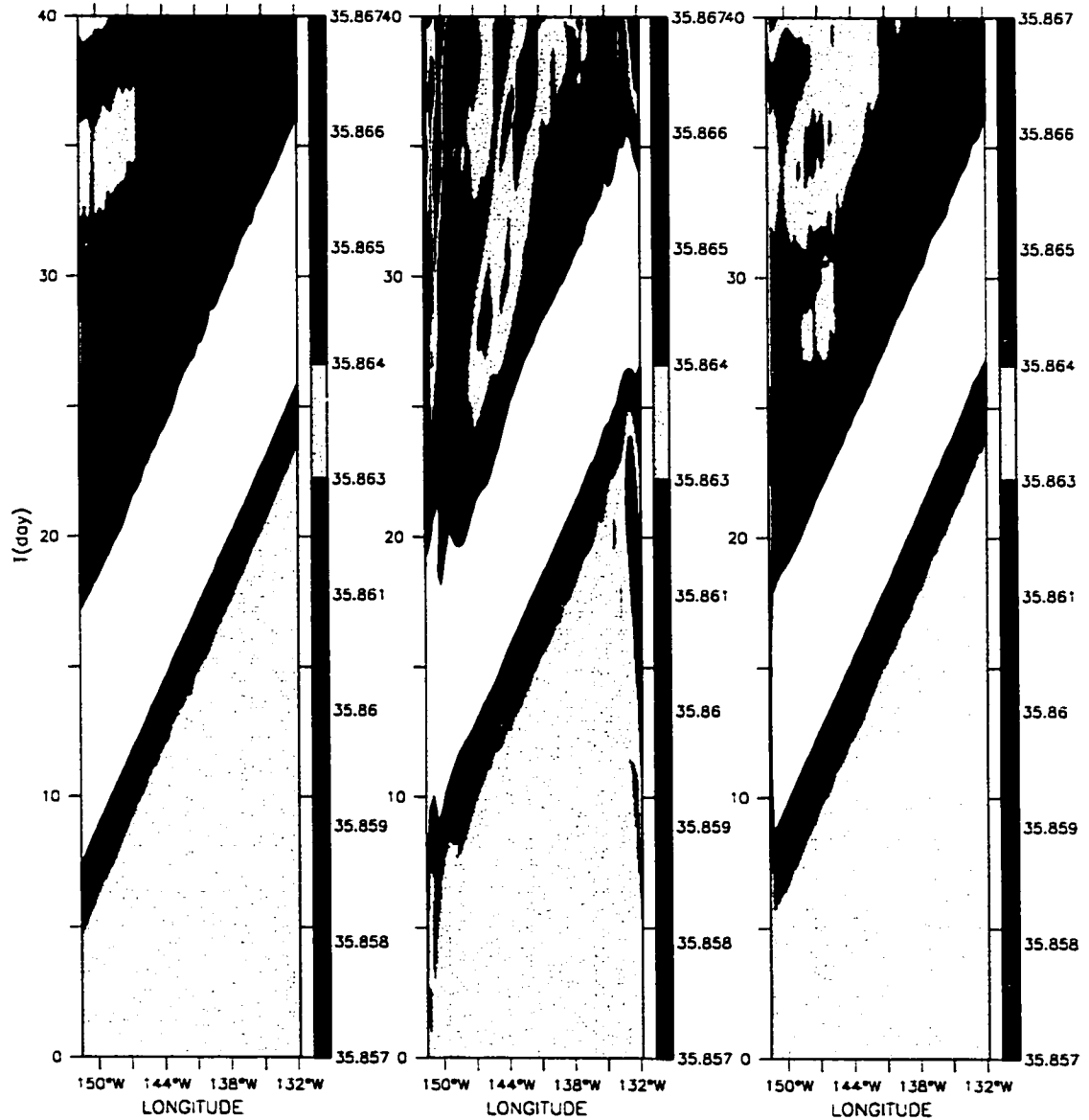


Figure 10: Time series plot of salinity along the equator of the coarse mesh domain run with the fine mesh resolution (left), NCOM-NCOM coupling with Orlanski boundary conditions (middle), and NCOM-NCOM coupling with NMOBC's.

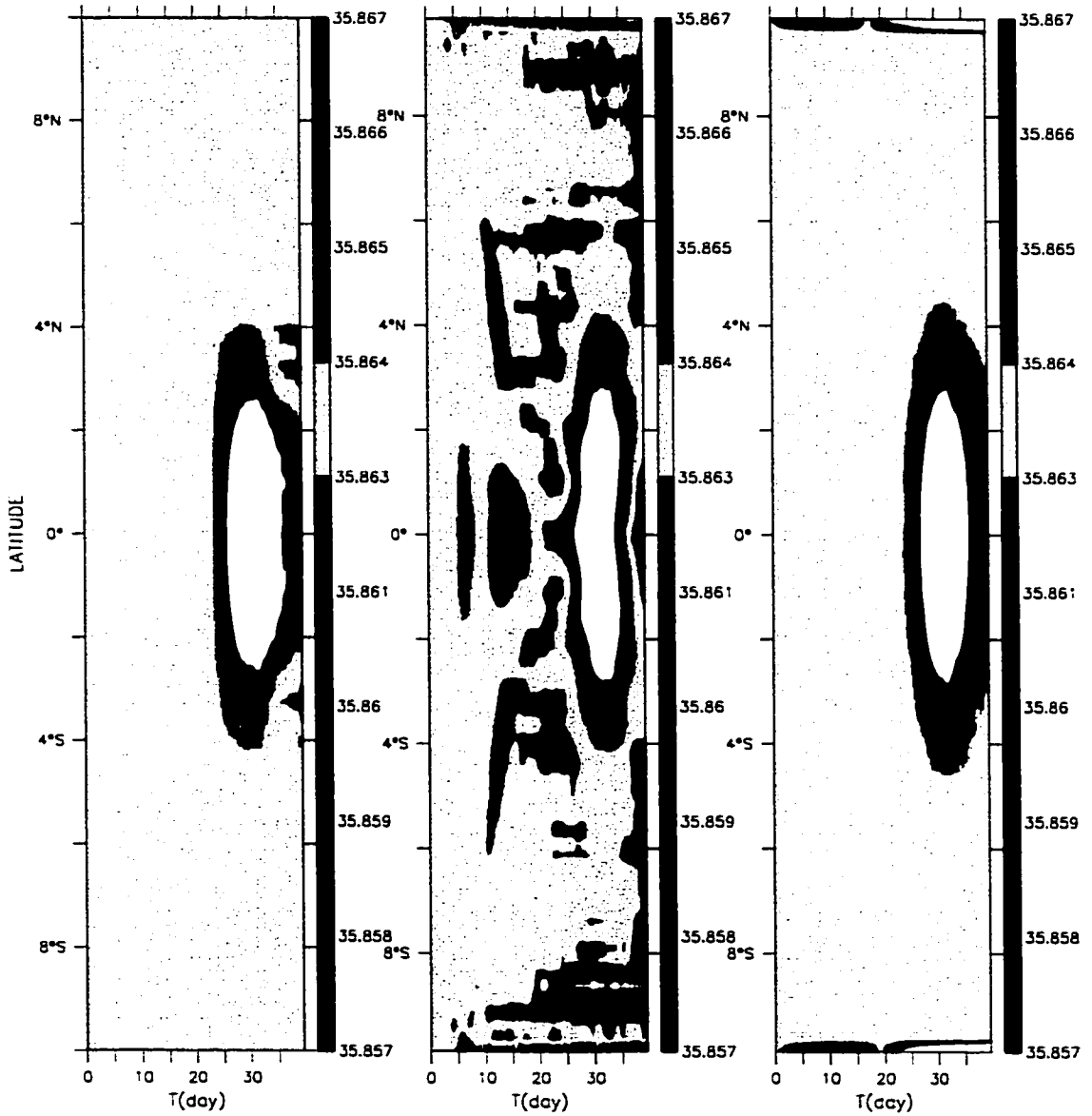


Figure 11: Time series plot of salinity along 132°W of the coarse mesh domain run with the fine mesh resolution (left), NCOM-NCOM coupling with Orlanski boundary conditions (middle), and NCOM-NCOM coupling with NMOBC's.

corresponding eigenvectors, and the remaining 33 modes of the fine mesh are allowed to follow a basic open boundary condition without any influence of the coarse mesh.

The NMOBC's have to be carried out a little differently in a coupling case than a nesting case. In the nesting case Camerlengo and O'Brien (1980) is used to calculate the phase speed of the baroclinic variables. In the coupling case better results are given if the phase speed of baroclinic velocities are calculated from the associated eigenvalues. The eigenvalues associated with the normal modes are given as $\lambda = \frac{1}{gh} = \frac{1}{c^2}$, therefore the phase speed is easily calculated. Also, in this case, the phase speeds are never negative so the phase speed always shows an outgoing wave. This actually helps the solution, as could be predicted from results reported by Durran et al. (1993). Durran et al. states that constant values of phase speed produce less numerical boundary noise than values that vary. Even though Camerlengo and O'Brien (1980) use phase speed of 0.0 or 1.0, the value at a single point and a single mode could oscillate between the two extreme from one time step to the next creating boundary noise.

The baroclinic results for the Orlanski and NMOBC cases are differenced from the baroclinic results of the coarse mesh run at the fine mesh resolution. These results are plotted in Figures 4-9 for days 10, 20, 30, and 40 for level 3 (~32 m depth). It can be seen from these figures that the interior solution for the two fine mesh cases are very similar; however, the results near the boundary are very different. The Orlanski solutions contain boundary noise that propagates into the interior solution. This does not happen in the NMOBC solution. The noise in the Orlanski solution is most likely a result of the noise produced because by density mismatches caused by the vertical interpolation

scheme used in the boundary values. This mismatch produces strong density gradients at the boundary, which induces opposing velocities only one grid spacing apart. This is seen in animations of the solution. This gives a very strong argument for the use of normal modes in coupling situations. With the use of vertical normal modes filling is not needed and the vertical information is passed more accurately.

The edge effects in the NMOBC salinity results are most likely the result of an error in the coding. This effect was not present in early forms of the code, but attempts to find the error have not been successful. However, because the errors do not destroy the stability on the boundary they do not propagate into the interior. This is result of the numerical errors of the NMOBC scheme being separate from the physical errors.

The large differences in the interior solution between the coarse mesh model run at the fine mesh resolution and the results of the coupled fine mesh runs appear to be the results of the difference in the phase speeds of the incoming waves produced by the 6 level coarse mesh and the phase speed of the same wave on a finer mesh. On the coarse mesh the phase speeds of the barotropic mode and the first two baroclinic-modes are 49.5585, 1.3945, and 0.7223 m/s respectively. On the fine mesh the phase speeds of the barotropic mode and the first two baroclinic-modes are 49.4969, 1.3790, and 0.6904 m/s respectively. Although the differences between these phase speeds are small, they are significant enough to impose a wave that propagates at a different speed than if the entire calculation was done on the finer mesh.

Another way of looking at the numerical boundary error produced with Orlanski or NMOBC's is to look at time series plots (Figures 10-11). Here two 1-D slices for salinity in the horizontal at 96 m depth are plotted showing results of the coarse mesh run

at the fine mesh resolution, the fine mesh using Orlanski radiation boundary conditions, and the fine mesh using NMOBC's. A slice along the equator of the fine mesh (Figure 10) shows a dominate Kelvin wave propagating through the domain, but it also shows the numerical error propagating off of the eastern and western boundary in the Orlanski case. This error is not present in the NMOBC case. Also, a slice near the eastern boundary of the fine mesh at 132°W and perpendicular to the eastern boundary shows numerical noise in the Orlanski case but not in the NMOBC case.

3.3 Gaussian Perturbation – NLOM Coupled to NCOM

In this test case, the coarse mesh solution is obtained from a six layer, hydrodynamic Naval Layered Ocean Model (NLOM) with the same horizontal grid as the previous coarse mesh model, equal thickness layers, and a 28-minute time step. Because this is a layered model, the physics of the model are quite different from the NCOM (see Appendix B for the NLOM model equations). Yet, it is often attractive to use a large-scale layered model in the deep ocean because of the capabilities of the layered system, while sigma level models work better in coastal regions where topography is variable and vertical density and current structure varies rapidly. This makes the coupling of these two types of models a desirable proposition. Yet, vertically interpolating NLOM variables to the NCOM vertical grid introduces a large source of noise on the NCOM grid. This is where normal modes are helpful. As shown in Appendix B, the vertical normal modes of the NCOM and the NLOM are identical. This supplies physical means to couple these differing models. In addition, Lighthill (1969) gives a more precise and

simpler calculation for the matrix, A , in equation (10) for a layered model. A is formed by

$$A_{jk} = \frac{gH_j \rho_{\min(j,k)}}{\rho_j} \quad (23)$$

where j and k are the matrix indices, g is gravity, H_j is the layer thickness of layer j , and ρ_j is the density of layer j . As in the previous section, the NMOBC's radiation portion are applied only to the first six levels and open boundary conditions are applied to the remaining 33 levels of the fine mesh NCOM, and the eigenvalues are used to provide the phase speed.

In this test case the fine mesh model is identical to the model in the previous section. The source of the coarse mesh boundary conditions is the only set-up difference between section 3.2 and section 3.3. For the Orlanski case, the input temperature and salinity are interpolated from values calculated from the Brydon et al. (1999) equation of state where density is known from the NLOM results and temperature is set to be a constant equal to 20°C for all layers. The NMOBC case uses the Brydon et al. results, but the vertical interpolation is not completed.

The NMOBC and Orlanski cases are again compared to the coarse mesh run on the fine mesh horizontal grid and 40-levels which was presented in the previous section (Figures 12-17). Like the coupled NCOM to NCOM case, the interior solutions for the two runs are similar, but again the Orlanski case has boundary errors that propagate into the interior. In this test case for the NMOBC's, the coarse mesh does not significantly influence the temperature and salinity because the modal values are too dissimilar between the NLOM and NCOM grids. Therefore, the model relaxes to temperature and

salinity values that are consistent with the baroclinic velocity structure. This is not an unusual idea; current techniques used to couple the NLOM to the NCOM do not always take into account the temperature and salinity. In these techniques, either the temperature and salinity are not forced at all, or the temperature and salinity are forced using climatological values from Levitus data.

Comparing the results of the coupled NCOM case to the coupled NLOM case reveal the differences between forcing a model with input from a model with the same or differing physics. As previously discussed, the coupled NCOM case shows phase speed error in the interior solution. The coupled NLOM case do not show phase speed errors but instead show magnitude errors, especially in u-velocities. This is a result of the phase speeds being more accurate with Lighthill's eigenvector calculation.

Time series plots of U-Velocity at 96 m depth for this test case also reveal the propagating numerical error in the Orlanski solution (Figures 18-19). U-Velocity is plotted instead of salinity because the velocity is calculated on the NLOM grid while the salinity has to be calculated from density. The NMOBC case is clean of propagating numerical error originating at the boundaries.

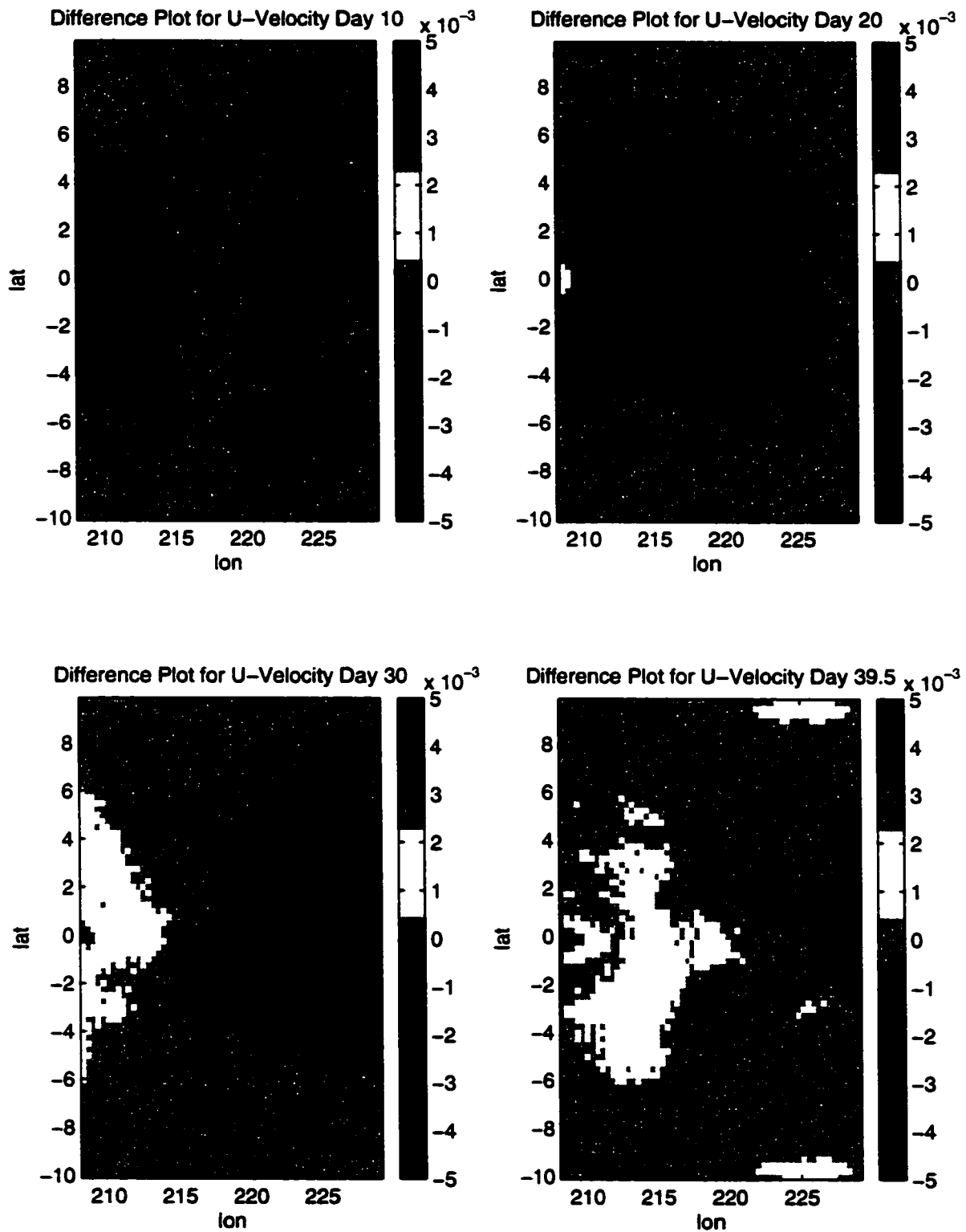


Figure 12: Difference plot for level 3 U-Velocity of the coarse mesh NCOM run at the fine mesh resolution and the NMOBC solution for the coupled NLOM to NCOM fine mesh at days 10, 20, 30, and 40.

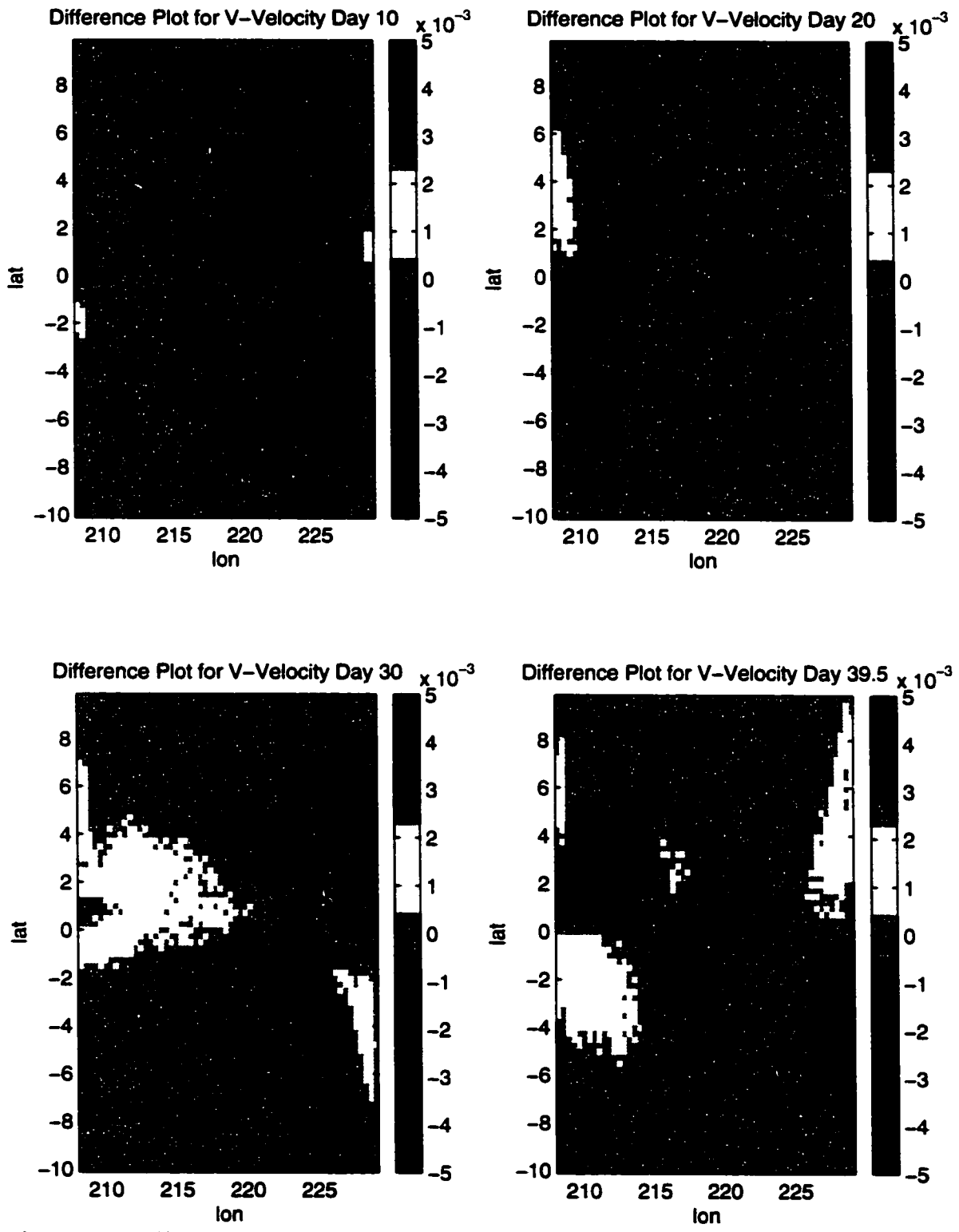


Figure 13: Difference plot for level 3 V-Velocity of the coarse mesh NCOM run at the fine mesh resolution and the NMOBC solution for the coupled NLOM to NCOM fine mesh at days 10, 20, 30, and 40

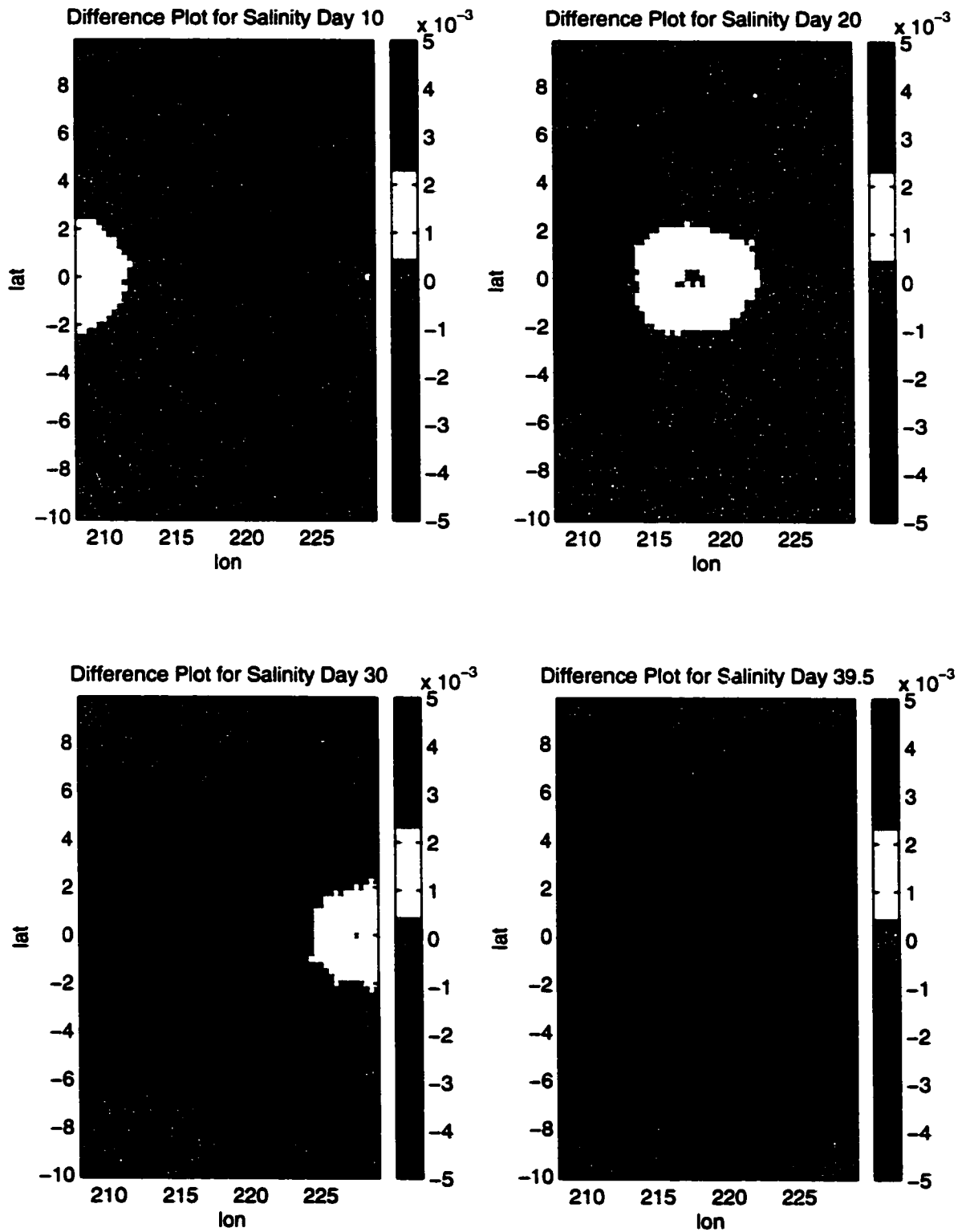


Figure 14: Difference plot for level 3 Salinity of the coarse mesh NCOM run at the fine mesh resolution and the NMOBC solution for the coupled NLOM to NCOM fine mesh at days 10, 20, 30, and 40.

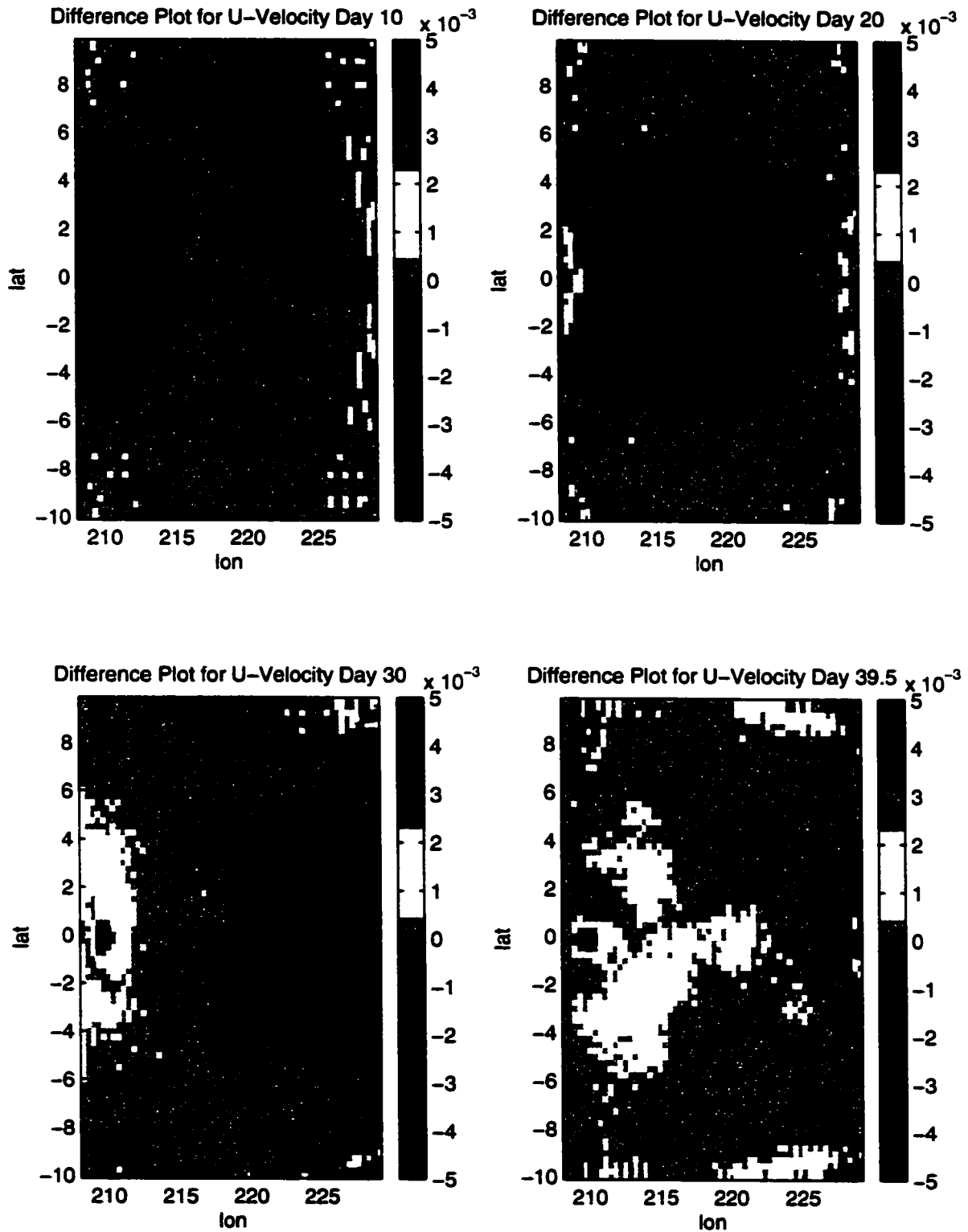


Figure 15: Difference plot for level 3 U-Velocity of the coarse mesh NCOM run at the fine mesh resolution and the Orlandi solution for the coupled NLOM to NCOM fine mesh at days 10, 20, 30, and 40.

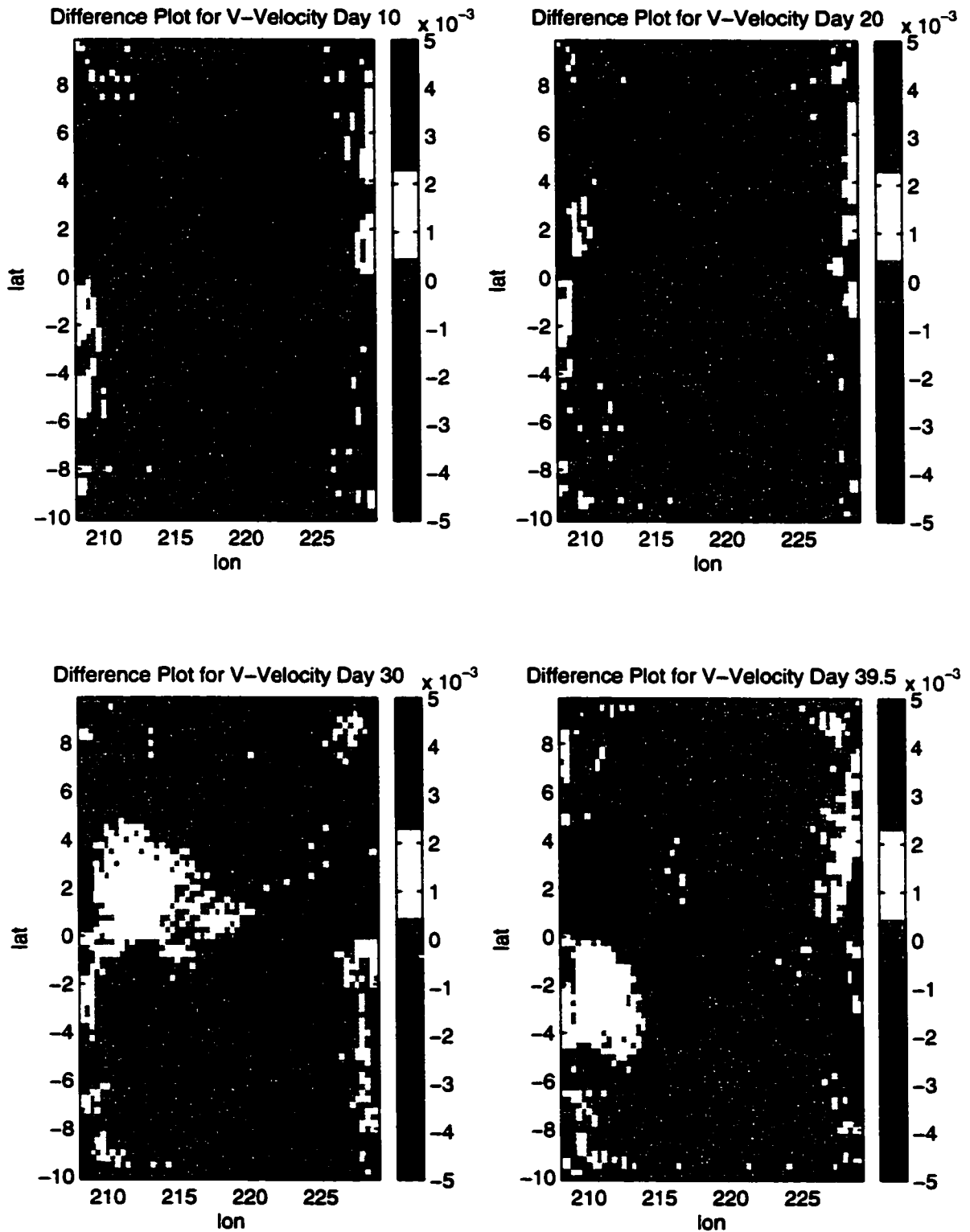


Figure 16: Difference plot for level 3 V-Velocity of the coarse mesh NCOM run at the fine mesh resolution and the Orlanski solution for the coupled NLOM to NCOM fine mesh at days 10, 20, 30, and 40.

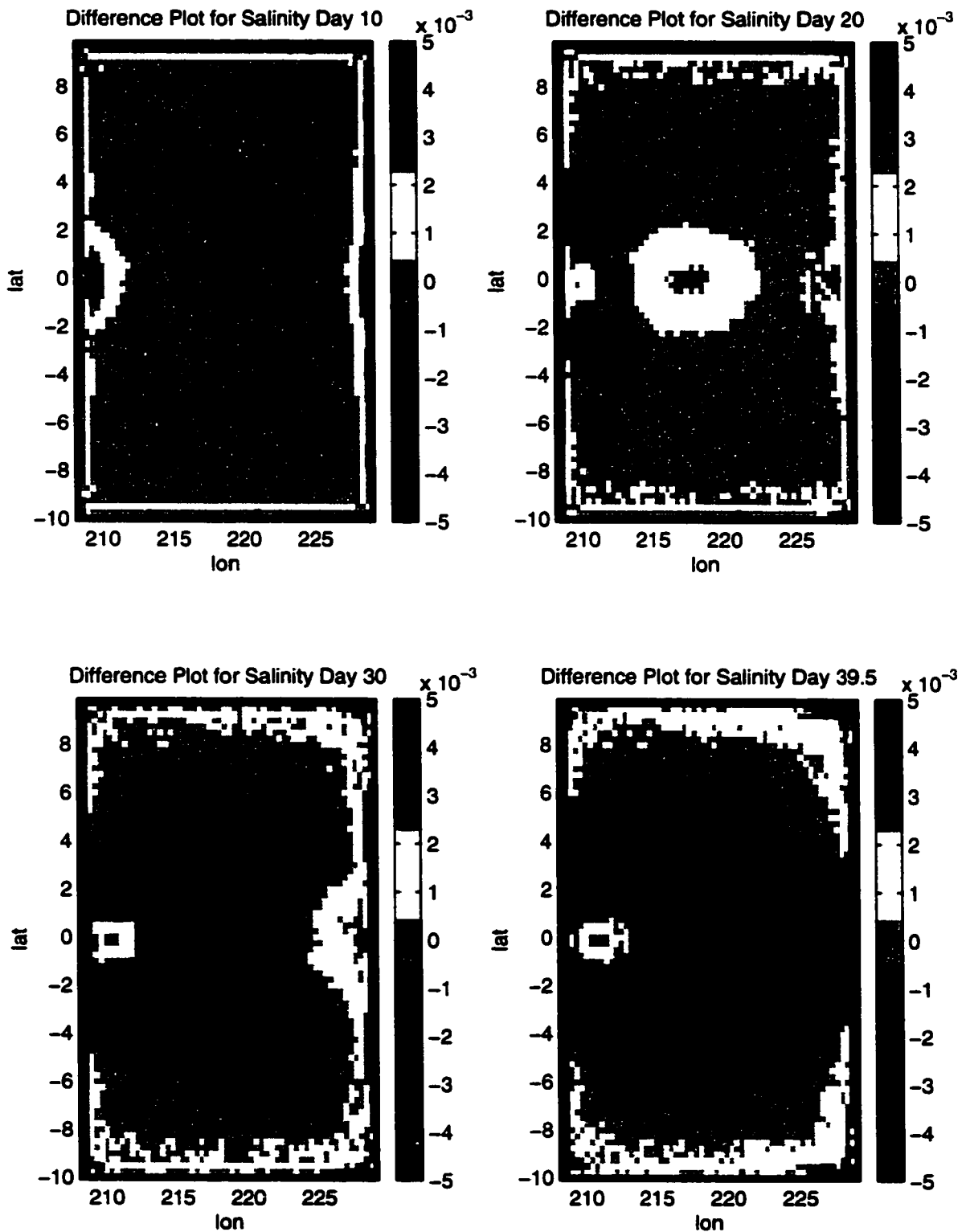


Figure 17: Difference plot for level 3 Salinity of the coarse mesh NCOM run at the fine mesh resolution and the Orlanski solution for the coupled NLOM to NCOM fine mesh at days 10, 20, 30, and 40.

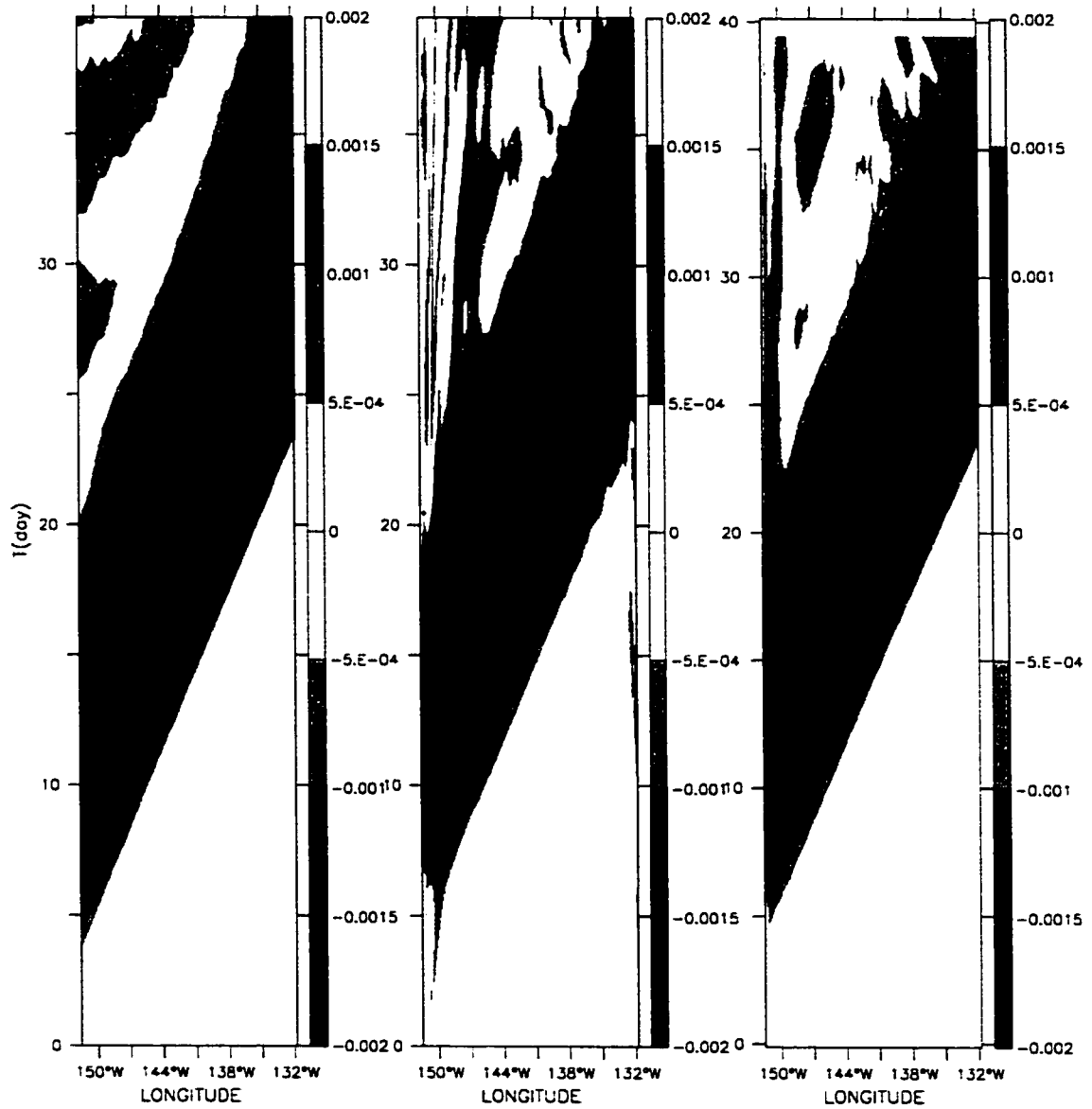


Figure 18: Time series plot of u -velocity along the equator of the coarse mesh domain run with the fine mesh resolution (left), NLOM-NCOM coupling with Orlanski boundary conditions (middle), and NLOM-NCOM coupling with NMOBC's.

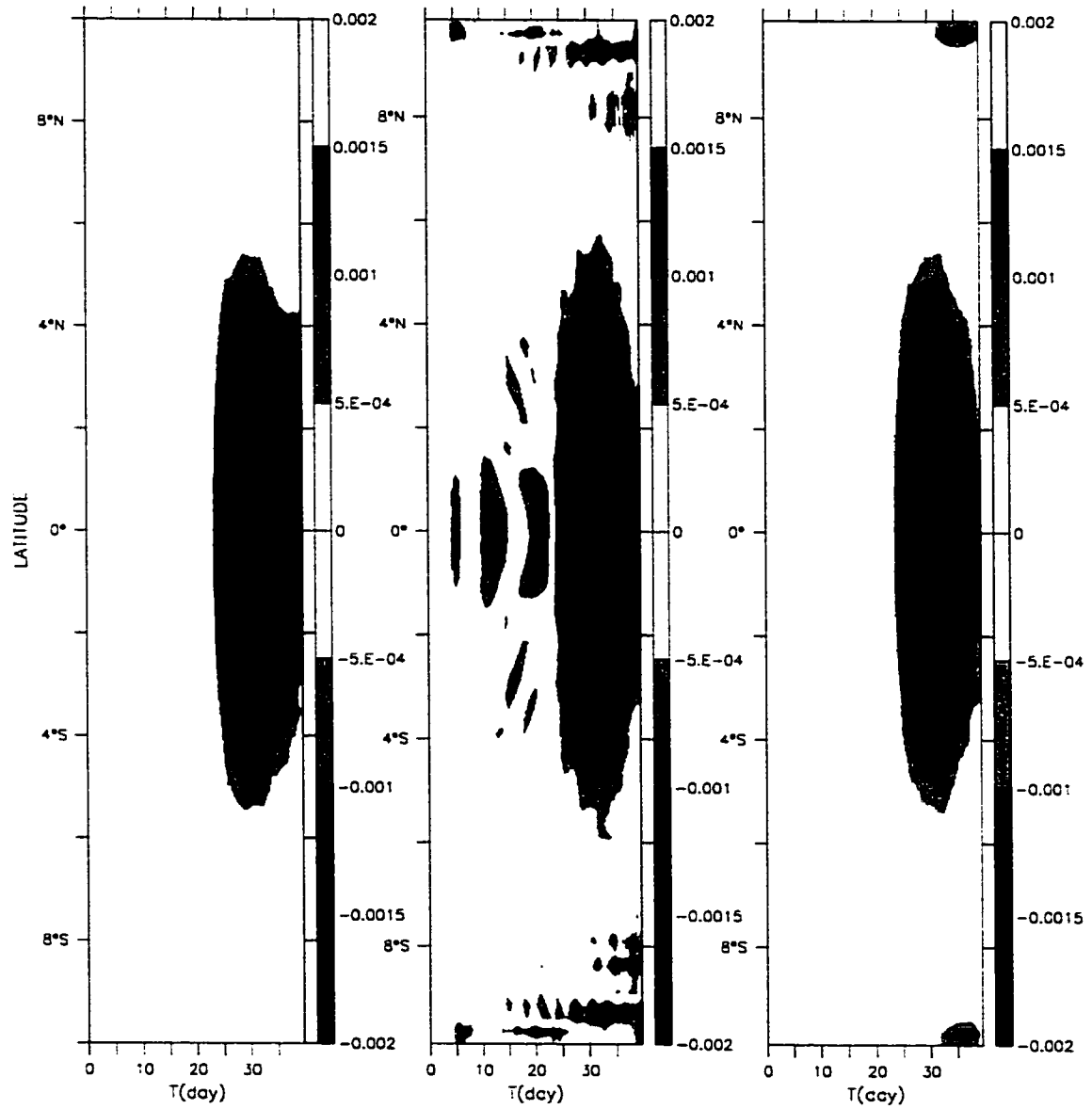


Figure 19: Time series plot of u-velocity along 132°W of the coarse mesh domain run with the fine mesh resolution (left), NLOM-NCOM coupling with Orlanski boundary conditions (middle), and NLOM-NCOM coupling with NMOBC's.

4. CONCLUSIONS

The results given in the previous sections demonstrate that normal mode open boundary conditions are a viable alternative to the commonly used Orlanski radiation boundary condition. This is especially true when the linkage requires vertical interpolation between the coarse and fine mesh in a coupling situation. This study was carried out in minimal flow situations. The low velocity values contribute to the noise in the radiation solutions. Yet, the NMOBC's handle low velocity situations with minimal numerical noise. Because radiation boundary conditions appear to have better results in situations of faster flow, it is reasonable to predict that the NMOBC's will also perform well under these conditions.

It should be noted that normal modes in their theoretical calculation assume that the ocean floor is flat. That necessity was taken into consideration when the previously discussed test cases were developed. It is unclear from this study how "flat" the bottom is required to be in the proximity of the boundary to apply NMOBC's. However, a slight modification to normal mode theory by Charney and Flierl (1981) allows non-flat bottoms. This modification may prove to be an improvement to NMOBC's in the future if flatness of bottom appears to be a hindrance to NMOBC's further development.

A benefit to using NMOBC's is the separation of numerical errors from physical errors. Because the modes are handled individually it can be easily found if the modes on

each grid match or if a mismatch in modal strength will produce aliasing. If aliasing has a potential of occurring, alternatives to the solution can be added to the code to limit the effect of the physical error. When the modes are not handled separately, the physical mismatch between the coupled models is disguised as numerical error.

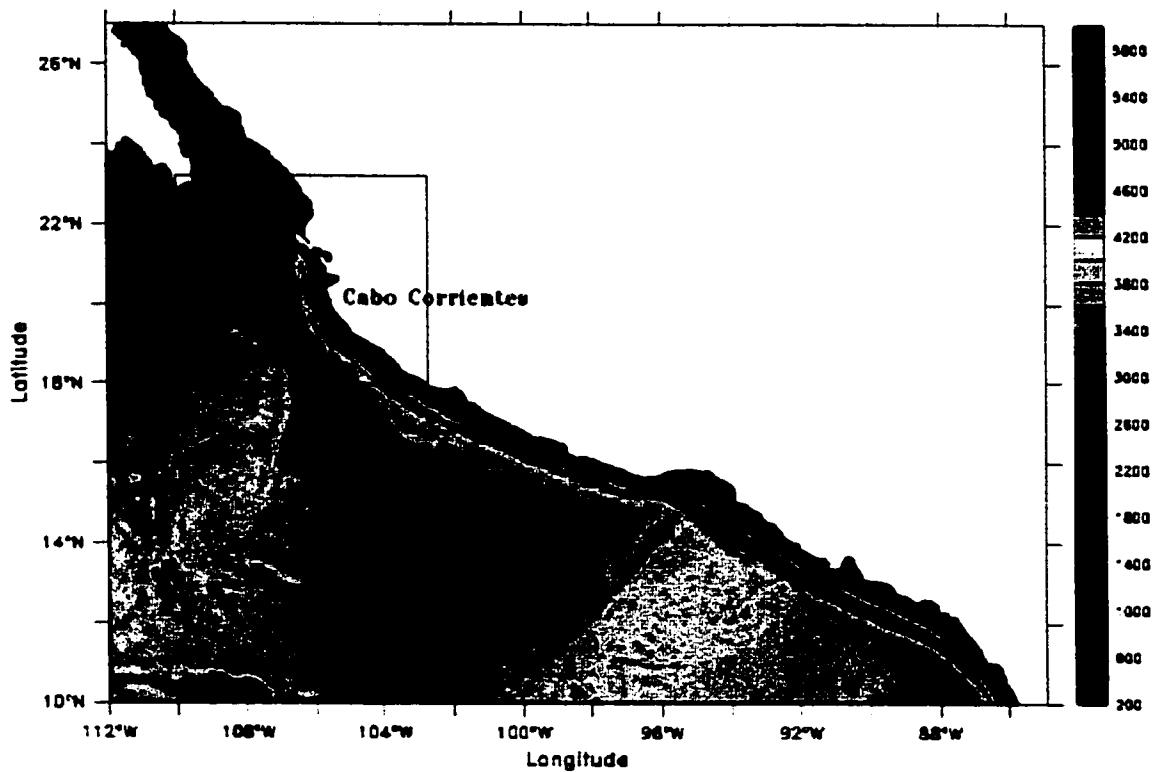


Figure 20: Bottom topography of coarse mesh grid proposed for future work. Inner box represents location of proposed fine mesh.

5. FUTURE WORK

Further studies to see how robust this method is are currently being developed. The study, currently being proposed, looks at eddy formation at Cabo Corrientes, Mexico (Figure 20). Eddies in this region are generated when a coastally trapped wave passes the cape at Cabo Corrientes. Zamudio (2001) showed that these eddies are the result of the intensity of the coastally trapped wave and the radius of curvature of the cape itself. Because the eddies are not a result of bottom topography or wind, new complexities can be added one by one to investigate the effect on the NMOBC's. Such complexities to be added include non-equal layer/level thicknesses, realistic thermocline structure, and realistic bottom topography. Plus, looking at eddies tests the NMOBC's with non-normal flow impacting the boundary.

APPENDIX A

NORMAL MODE DERIVATION OF NCOM EQUATIONS

Using the method put forth by Philander (1990), the normal modes of the NCOM model equations are here derived. The NCOM equations are as given in equations (1) to (8). To perform the normal mode calculation the model equations first need to be reduced to five equations. The reduction begins by examining the time dependence of the equation of state, (8)

$$\frac{d\rho}{dt} = \left. \frac{\partial\rho}{\partial T} \right|_S \frac{dT}{dt} + \left. \frac{\partial\rho}{\partial S} \right|_T \frac{dS}{dt} = -\alpha\rho_0 \frac{dT}{dt} + \beta\rho_0 \frac{dS}{dt}. \quad (1A)$$

Expanding the material time derivatives as

$$\rho_0^{-1} \left(\frac{\partial\rho}{\partial t} + \bar{\nabla} \cdot (\bar{v}\rho) \right) = -\alpha \left(\frac{\partial T}{\partial t} + \bar{\nabla} \cdot (\bar{v}T) \right) + \beta \left(\frac{\partial S}{\partial t} + \bar{\nabla} \cdot (\bar{v}S) \right) \quad (3A)$$

allows equations (6) and (7) to be substituted to obtain the form

$$\rho_0^{-1} (\rho_t + \bar{\nabla} \cdot (\bar{v}\rho)) = -\alpha [QT + \nabla_h(A_H \nabla_h T) + (K_H T_z)_z + Q_r \gamma_z] + \beta [QS + \nabla_h(A_H \nabla_h S) + (K_H S_z)_z] \quad (4A)$$

where the subscript z equals $\partial/\partial z$ and the subscript t equals $\partial/\partial t$.

By again using equation (1A) it can be shown that

$$\rho_0^{-1} \nabla_h(A_H \nabla_h \rho) = -\alpha \nabla_h(A_H \nabla_h T) + \beta \nabla_h(A_H \nabla_h S) \quad (5A)$$

and

$$\rho_0^{-1} (K_H \rho_z)_z = -\alpha (K_H T_z)_z + \beta (K_H S_z)_z. \quad (6A)$$

Substituting (5A) and (6A) into (4A) gives a prognostic equation for density

$$\rho_0^{-1} \rho_t = -\rho_0^{-1} \bar{\nabla} \cdot (\bar{v} \rho) + Q(-\alpha T + \beta S) + \rho_0^{-1} \nabla_h (A_H \nabla_h \rho) + \rho_0^{-1} (K_H \rho_z)_z - \alpha Q \gamma_z \quad (7A)$$

that can replace equations (6) to (8). Equation (7A) along with equations (1) to (4) are the reduced set of equations from which to solve for the normal modes.

The next step in forming the normal mode equation is to linearize the five reduced equations. When linearizing, the ocean is assumed to be in its basic state, motionless, and motion and density variations are small perturbations to the basic state. The vertical variation in density is the square Brünt – Väisälä frequency: $N^2 = -g\rho_0^{-1} \rho_z$, where ρ_0 is set as a model constant. Let $K_M = K_H = A/N^2$. Also substitute in correct forms of F_u and F_v (Martin et al., 1998); $F_u = \nabla_h (A_M \nabla_h u)$ and $F_v = \nabla_h (A_M \nabla_h v)$, where A_M is the horizontal mixing coefficient. With these assumptions, the linearized form of the NCOM equations become

$$u_t - fv + \rho_0^{-1} p_x = Qu + \nabla_h (A_M \nabla_h u) + \left(\frac{A}{N^2} u_z \right)_z \quad (8A)$$

$$v_t + fu + \rho_0^{-1} p_y = Qv + \nabla_h (A_M \nabla_h v) + \left(\frac{A}{N^2} v_z \right)_z \quad (9A)$$

$$u_x + v_y + w_z = Q \quad (10A)$$

$$\rho g + p_z = 0 \quad (11A)$$

$$\rho_0^{-1} \rho_t - \frac{N^2 w}{\rho_0 g} = Q(-\alpha T + \beta S) + \rho_0^{-1} \nabla_h (A_H \nabla_h \rho) - \left(\frac{AN^2}{N^2 g} \right)_z - \alpha Q \gamma_z \quad (12A)$$

Further simplify these equations by letting Q equal zero and having a negligible effect from solar radiation. Note that $(AN^2 / N^2 g)_z = (A/g)_z = 0$.

With this form of the equations it is possible to solve for the normal modes as in Philander (1990). First, eliminate ρ by substituting (11A) into (12A) to obtain

$$p_z + N^2 w = \nabla_h(A_H \nabla_h p_z) \quad (14A)$$

For the normal mode decomposition apply a separation of variables to the simplified equations (8A) to (10A) and (14A) of the form

$$u = \sum U_m(x, y, t) R_m(z) \quad (15A)$$

$$v = \sum V_m(x, y, t) R_m(z) \quad (16A)$$

$$p = \sum \eta_m(x, y, t) R_m(z) \quad (17A)$$

$$w = \sum W_m(x, y, t) S_m(z) \quad (18A)$$

Substitution yields

$$U_x R - f V R + \rho_0 \eta_x R = \left(\frac{A}{N^2} U R_z \right)_z \quad (19A)$$

$$V_x R + f U R + \rho_0 \eta_y R = \left(\frac{A}{N^2} V R_z \right)_z \quad (20A)$$

$$U_x R + V_y R + W S_z = 0 \quad (21A)$$

$$\eta_x R_z + N^2 W S = \nabla_h(A_H \nabla_h \eta R_z) \quad (22A)$$

where the subscript m has been dropped. By rearranging (21A) to isolate the dependence on the z coordinate one finds

$$\frac{U_x + V_y}{-W} = \frac{S_z}{R} = -\lambda \quad (23A)$$

Therefore, if $\lambda = 1/gh$

$$R = -gh S_z \quad (24A)$$

By separating the z-dependence in (19A) one obtains

$$\frac{U_t - fV + \eta_x}{AU} = \frac{1}{R} \left(\frac{R_z}{N^2} \right)_z = -\frac{1}{gh}. \quad (25A)$$

This gives the separated equations

$$U_t - fV + \eta_x = -AU / gh \quad (26A)$$

and

$$\left(\frac{R_z}{N^2} \right)_z = -R / gh. \quad (27A)$$

To separate (22A) divide by N^2 , apply $\partial / \partial z$ and substitute in equation (21A) to obtain

$$\eta_t \left(\frac{R_z}{N^2} \right)_z - R(U_x + V_y) = \nabla_h \left(A_H \nabla_h \eta \left(\frac{R_z}{N^2} \right)_z \right). \quad (28A)$$

A separation of variables then yields

$$\frac{U_x + V_y}{\eta_t - \nabla_h (A_H \nabla_h \eta)} = \frac{1}{R} \left(\frac{R_z}{N^2} \right)_z = -\frac{1}{gh}. \quad (29A)$$

Equations (26A), along with the corresponding V form, and (29A) represent

the (x, y, t) normal mode equations:

$$U_t - fV + g\eta_x = -AU / gh \quad (30A)$$

$$V_t + fU + g\eta_y = -AV / gh \quad (31A)$$

$$\eta_t - \nabla_h (A_H \nabla_h \eta) = -gh(U_x + V_y) \quad (32A)$$

The vertical mode equation related to the vertical velocity is formed by combining

equations (24A) and (27A) to get

$$\left(\frac{S_z}{N^2} \right)_z + \frac{S_z}{gh} = 0. \quad (33A)$$

This has the general solution

$$S_z + \frac{N^2}{gh} S = c \quad (34A)$$

for which the arbitrary constant, c , can be chosen to have the particular solution $c = 0$

without a loss of generality. This differential equation is of the Sturm-Liouville form and

can be solved via standard numerical methods. Likewise, the vertical mode equation related to the density and horizontal velocities is given by (27A) and is written in Sturm-Liouville form as

$$\frac{\partial}{\partial z} \left(\frac{1}{N^2} \frac{\partial R}{\partial z} \right) + \frac{1}{gh} R = 0. \quad (35A)$$

This is the form of the vertical normal mode equation used to calculate the eigenvalues and eigenvectors for the open boundary conditions in the presented method.

APPENDIX B

NORMAL MODE DERIVATION OF NLOM EQUATIONS

The normal modes for the NRL Layered Ocean Model (NLOM) are derived similarly to the NCOM case. The current NLOM is a descendent of the layer model by Hurlburt and Thompon (1980). It has significant enhancements that are discussed in Wallcraft (1991), Wallcraft and Moore (1997), and Moore and Wallcraft (1998). The NLOM is available reduced gravity and finite depth versions. Also, the NLOM can be run in either a hydrodynamic mode, which is spatially and temporally constant density within each layer, or a thermodynamic mode, which has density varying spatially and temporally in each layer, i.e. density is a prognostic variable.

The vertically integrated equations of motion for the NLOM are of the form:

$$\begin{aligned} \frac{\partial \bar{V}_k}{\partial t} + (\nabla \cdot \bar{V}_k + \bar{V}_k \cdot \nabla) \bar{V}_k + \hat{k} \times f \bar{V}_k = -h_k \sum_{l=1}^n G_H \nabla (h_l - H_l) \\ + \max(0, \omega_k) \bar{v}_{k+1} - (\max(0, -\omega_k) + \max(0, \omega_{k-1})) \bar{v}_k + \max(0, -\omega_{k-1}) \bar{v}_{k-1} \end{aligned} \quad (1B)$$

$$+ (\bar{\tau}_{k-1} - \bar{\tau}_k) / \rho_0 + A_H h_k \nabla^2 \bar{v}_k$$

$$\frac{\partial h_k}{\partial t} + \nabla \cdot \bar{V}_k = \omega_k - \omega_{k-1} \quad (2B)$$

where

h_k = k -th layer thickness

\bar{v}_k = k -th layer velocity

$$\bar{V}_k = h_k \bar{v}_k$$

$H_k = k$ -th layer thickness at rest

$$H_n = D(x, y) - \sum_{l=1}^{n-1} H_l$$

$D(x, y) =$ total depth of the ocean at rest

$f =$ coriolis parameter

$A_H =$ coefficient of horizontal eddy viscosity

$\rho_k = k$ -th layer density, constant in space and time

$$G_{kl} = \begin{cases} g & \text{for } l \leq k \\ g - g(\rho_l - \rho_k) / \rho_0 & \text{for } l > k \end{cases}$$

$$\bar{\tau}_k = \begin{cases} \bar{\tau}_w & \text{for } k = 0 \\ C_k \rho_0 |\bar{v}_k - \bar{v}_{k+1}| (\bar{v}_k - \bar{v}_{k+1}) & \text{for } k = 1 \dots n-1 \\ C_b \rho_0 |\bar{v}_n| \bar{v}_n & \text{for } k = n \end{cases}$$

$C_k =$ coefficient of interfacial friction

$C_b =$ coefficient of interfacial friction

$\bar{\tau}_w =$ wind stress

$$\omega_k = \begin{cases} 0 & \text{for } k = 0, n \\ \max(0, \omega_k^+) - \max(0, \omega_k^-) - h_k \hat{\omega}_k & \text{for } k = 1 \dots n-1 \end{cases}$$

$$\omega_k^+ = \tilde{\omega}_k \frac{h_k^+}{4} \left(\frac{1}{h_k^-} - \frac{1}{h_k^+} \right)$$

$$\omega_k^- = \tilde{\omega}_k \frac{h_k}{4} \left(\frac{1}{h_k^- + h_k^+ - h_k} - \frac{1}{h_k^+} \right)$$

$$\hat{\omega}_k = \frac{\iint (\max(0, \omega_k^+) - \text{mask}(0, \omega_m^-))}{\iint H_k}$$

$\tilde{\omega}_k$ = k -th interface reference vertical mixing velocity

h_k^+ = k -th layer thickness at which entrainment starts

h_k^- = k -th layer thickness at which detrainment starts.

For the purpose of forming the normal modes the mixing terms in equations (1B) and (2B) will be ignored because these effects are usually local and relatively small scale. Also, because the normal modes are linear approximations, boundary regions where strong mixing occurs are not appropriate locations for the normal mode boundary conditions to be applied.

It is desirable to have all the components involving velocity to be in transport form. Following the suggestion put forth by Hurlburt and Thompson (1980), the horizontal friction is rewritten as $A_H \nabla^2 \bar{V}_k$ instead of $A_H h_k \nabla^2 \bar{v}_k$. According to Hurlburt and Thompson, there were only small quantitative differences between the two forms in their study. The interfacial stress can also be rewritten in terms of transport, such that

$$\frac{(\bar{\tau}_{k-1} - \bar{\tau}_k)}{\rho_0} = \frac{1}{\rho_0} (C_k \rho_0 |\bar{v}_k - \bar{v}_{k+1}| (\bar{v}_k - \bar{v}_{k+1}))_z = \left(K_m \frac{\partial \bar{v}_k}{\partial z} \right)_z = \left(K_m \frac{\partial}{\partial z} \left(\frac{\bar{V}_k}{H_k} \right) \right)_z \quad (3B)$$

where the z subscripts are z -derivatives.

Next, the perturbation equations are formed assuming that the ocean is in its basic state, motionless, and motion and height variations are small perturbations to the basic state, such that,

$$h_k = h'_k + H_k \quad (4B)$$

$$\bar{V}_k = (h'_k + H_k)(v'_k + \bar{v}_k) = h_k v'_k = \bar{V}'_k \quad (5B)$$

Linearize and rewrite (1B) and (2B) as

$$\frac{\partial \vec{V}'_k}{\partial t} + \hat{k} \times f \vec{V}'_k = -H_h \sum_{l=1}^n G_{kl} \nabla H'_l + \left(K_m \frac{\partial}{\partial z} \frac{\vec{V}'_k}{H_k} \right)_z + A_H \nabla^2 \vec{V}'_k \quad (6B)$$

$$\frac{\partial H'_k}{\partial t} + \nabla \cdot \vec{V}'_k = 0 \quad (7B)$$

To form the normal mode equations let $K_m = A/N^2$. Then apply a separation of variables of the form (dropping the primes and the layer indices)

$$\vec{V} = \sum \vec{V}_m(x, y, t) R_m(z) \quad (8B)$$

$$h = \sum W_m(x, y, t) S_m(z) \quad (9B)$$

to equations (6B) and (7B) to yield

$$R \vec{V}_t + \hat{k} \times f R \vec{V} = H \sum G \nabla S W + \left(\frac{A}{N^2} \frac{1}{H} R_z \vec{V} \right)_z + A_H \nabla^2 R \vec{V} \quad (10B)$$

$$S W_t + R(\nabla \cdot \vec{V}) = 0 \quad (11B)$$

for each mode m.

Take $\partial/\partial t$ of (10B) and substitute (11B) into the new equation to form

$$R \vec{V}_{tt} + \hat{k} \times f R \vec{V}_t = -H \sum G \nabla R(\nabla \cdot \vec{V}) + \frac{A}{H} \vec{V}_t \left(\frac{R_z}{N^2} \right)_z + R A_H \nabla^2 \vec{V}_t \quad (12B)$$

Separate the horizontal and vertical components of (12B) such that

$$\frac{\vec{V}_{tt} + \hat{k} \times f \vec{V}_t + H \sum G \nabla (\nabla \cdot \vec{V}) - A_H \nabla^2 \vec{V}_t}{\frac{A}{H} \vec{V}_t} = \frac{1}{R} \left(\frac{R_z}{N^2} \right)_z \quad (13B)$$

Set (13B) equal to $-\lambda = -1/gh$ and form the separated vertical normal mode equation

$$\left(\frac{R_z}{N^2} \right)_z + \frac{1}{gh} R = 0 \quad (14B)$$

which is the same as equation (27A) for the NCOM.

Separating the horizontal components from the vertical components in equation

(11B) gives

$$\frac{\nabla \cdot \vec{V}}{W_i} = \frac{S}{R} = -\frac{1}{gh} \quad (15B)$$

Therefore, the horizontal normal modes for the NLOM are

$$\vec{V}_u + \hat{k} \times f \vec{V} + H \sum G \nabla (\nabla \cdot \vec{V}) - A_H \nabla^2 \vec{V}_i + \frac{A}{ghH} \vec{V}_i = 0 \quad (16B)$$

$$(\nabla \cdot \vec{V}) + \frac{1}{gh} W_i = 0 \quad (17B)$$

And the vertical normal mode for the layer thickness is

$$\left(\frac{S_z}{N^2} \right)_z + \frac{1}{gh} S = 0 \quad (18B)$$

APPENDIX C
CALCULATION OF δs

To excite a first baroclinic mode wave in the NCOM a salinity perturbation is calculated as follows. First, R in equation (35A) is set equal to a pressure perturbation, p' , N equal to a constant, and assuming a rigid lid for simplification purposes a solution to the Sturm-Liouville PDE is

$$p'(z) = \cos(k\pi z/H) \quad (1C)$$

and

$$c_k = \frac{NH}{k\pi} = \sqrt{gh_k}. \quad (2C)$$

Since only the first baroclinic mode is of interest set $k=1$. To keep the results of this study comparable to that of Ginis et al. (1998) and Philander et al. (1984) set $c_1=1.4$ m/s. Thus with a maximum depth of $H=500$ m, the equivalent depth is $h_1=0.2$ m, and the Brunt-Väisälä frequency is $N = 8.8 \times 10^{-3} \text{ s}^{-1}$. From the hydrostatic approximation it can be shown that

$$\frac{dp'}{dz} = \rho'g. \quad (3C)$$

Using this relation with (1C) gives

$$\rho'(z) = \frac{-\pi}{gH} \sin\left(\frac{\pi z}{H}\right). \quad (4C)$$

The equation of state calculation used in this study is the one put forward by Brydon et al. (1999). In this calculation density and salinity are linearly related, so to a first approximation δs can be set equal to ρ' .

REFERENCES

- Alapaty, K., R. Mathur, and T. Odman, Intercomparison of spatial interpolation schemes for use in nested grid models, *Mon. Weather Rev.*, *126*, 243-249, 1998.
- Brydon, D., S. Sun, and R. Bleck, A new approximation of the equation of state for seawater, suitable for numerical ocean models, *J. Geophys. Res.*, *104*, 1537-1540, 1999.
- Camerlengo, A. J., and J. J. O'Brien, Open boundary conditions in rotating fluids, *J. Comput. Phys.*, *35*, 12-35, 1980.
- Charney J. G. and G. R. Flierl, Oceanic Analogues of Large-scale Atmospheric Motions, in *Evolution of Physical Oceanography: Scientific Surveys in Honor of Henry Stommel*, edited by B. A. Warren and C. Wunsch, The Massachusetts Institute of Technology, 504-548, 1981.
- Durrant, D. R., M. J. Yang, D. N. Slinn, and R. G. Brown, Toward more accurate wave-permeable boundary conditions, *Mon. Weather Rev.*, *121*, 604-620, 1993.
- Fox, A. D. and S. J. Maskell, Two-way interactive nesting of primitive equation ocean models with topography, *J. Phys. Oceanogr.*, *25*, 2977-2996, 1995.
- Gill, A. E., *Atmosphere-Ocean Dynamics*, pp.159-162, Academic Press, New York, 1982.
- Ginis, I., A. Richardson, and L. M. Rothstein, Design of a multiply nested primitive equation ocean model, *Mon. Weather Rev.*, *126*, 1054-1079, 1998.
- Hurlburt, H. E. and J. D. Thompson, A numerical study of loop current intrusions and eddy shedding, *J. Phys. Oceanogr.*, *10*, 1611-1651, 1980.
- Jensen, T. G., Open boundary conditions in stratified ocean models, *J. Marine Sys.*, *16*, 297-322, 1998.
- Kurihara, Y., G. J. Tripoli, and M. A. Bender, Design of a movable nested-mesh primitive equation model, *Mon. Wea. Rev.*, *107*, 239-249, 1979.
- Kürschner, R., Instabilities of protostellar cores. The influence of adaptive grids on

- instabilities of first protostellar cores, *Astron. Astrophys.*, 285, 897-902, 1994.
- Laugier, M., P. Angot, and L. Mortier, Nested grid methods for an ocean model: A comparative study, *Int. J. Numer. Meth. Fl.*, 23, 1163-1195, 1996.
- Lighthill, M. J., Dynamic response of the Indian Ocean to onset of the Southwest Monsoon, *Phil. Trans. Roy. Soc. London. A265*, 45-92, 1969.
- Martin, P. J., *A Description of the Navy Coastal Ocean Model Version 1.0*, NRL Report: NRL/FR/7322-00-9962, Naval Research Laboratory, Stennis Space Center, MS., 39 pp, 2000.
- Mellor, G. L., An equation of state for numerical models of oceans and estuaries, *Atmos. Oceanic. Technol.*, 8, 609-611, 1991.
- Moore, D. R. and A. J. Wallcraft, *Formulation of the NRL Layered Ocean Model in spherical coordinates*, NRL Report: NRL/CR/7323—96-0005, Naval Research Laboratory, Stennis Space Center, MS., 24 pp, 1998.
- Palma, E. D. and R. P. Matano, On the implementation of passive open boundary conditions for a general circulation model: The barotropic mode, *J. Geophys. Res.*, 103, 1998.
- Palma, E. D. and R. P. Matano, On the implementation of open boundary conditions for a general circulation model: The three-dimensional case, *J. Geophys. Res.*, 105, 8605-8627, 2000.
- Perkins, A. L. and L. F. Smedstad, Scale-related aspects of nested finite difference ocean models, *Theoret. Comput. Fluid Dynamics*, 10, 311-322, 1998.
- Philander, S. George, *El Niño, La Niña, and the Southern Oscillation*, pp. 160-167, Academic Press, Inc., New York, 1990.
- Philander, S. G. H., T. Yamagata, and R. C. Pacanowski, Unstable air-sea interactions in the tropics, *J. Atmos. Sci.*, 41, 604-613, 1984.
- Rochford, P. A. and P. J. Martin, *Boundary Conditions in the Navy Coastal Ocean Model*, NRL Report: NRL/FR/7330—01-9992, Naval Research Laboratory, Stennis Space Center, MS., 37 pp, 2001.
- Røed, L. P. and C. K. Cooper, Open boundary conditions in numerical ocean models, in *Advanced Physical Oceanographic Numerical Modelling*, edited by J. J. O'Brien, pp. 411-436, D. Reidel Publishing Company, Boston, 1986.
- Skamarock, W. C. and J. B. Klemp, Adaptive grid refinement for two-dimensional and three-dimensional nonhydrostatic atmospheric flow, *Mon. Wea. Rev.*, 121, 788-

804, 1993.

Spall, M. A. and W. R. Holland, A nested primitive equation model for oceanic applications, *J. Phys. Oceanogr.*, 21, 205-220, 1991.

Wallcraft, A. J., *The Navy Layered Ocean Model users guide*, NOARL Report 35, 21 pp, 1991.

Wallcraft, A. J. and D. R. Moore, The NRL Layered Ocean Model, *Parallel Computing*, 23, 2227-2242, 1997.

Zamudio-Lopez, L. F., *Mesoscale Variability Along the Southwest Coast of Mexico Induced by Oceanic and Atmospheric Remote Forcings*, Ph.D Dissertation, 95 pp., Florida State University, 2001.

Zhang, D., et al., A two-way interactive nesting procedure with variable terrain resolution, *Mon. Wea. Rev.*, 114, 1330-1339, 1986.

BIOGRAPHICAL SKETCH

Name: Andrea C. Mask.
Date of Birth: March 9, 1972.
Citizenship: United States.
Marital Status: Married.

Degrees: University of Southern Mississippi, **M.S., Physics and Mathematics**, 1994.
Senior Thesis Title: "Electric Field and Size Induced Configuration Transitions"

The Florida State University, **B.S., Physical Oceanography**, 1996.
Thesis Title: "Wind Driven Effects on the Yellow Sea Warm Current"

Awards and Honors: Naval Research Laboratory **Graduate Student Fellowship**, 1994-2000.
University of Southern Mississippi, **Cum Laude**, 1994.
University of Southern Mississippi, **Honors College**, 1990-1994.

Professional Experience:

(a) Publications: Mask, A. C., J. J. O'Brien, and R. Preller, 1998: **Wind-driven effects on the Yellow Sea Warm Current**. *J. Geophys. Res.*, 103, C13, 30,713-30,729.

(b) Meetings: Ocean Sciences, San Antonio, TX. 2000.

Sigma Coordinate Ocean Model Users Meeting, Bar Harbor, ME. 1999.

American Geophysical Union – Fall Meeting, San Francisco, CA. 1996.
Topic Title: "Wind Driven Effects on the Yellow Sea Warm Current".

Princeton Ocean Model Users Meeting, Princeton, NJ. 1996.

(c) Teaching: 1992-1993 **Laboratory Assistant**, University of Southern Mississippi, Physics and Astronomy Department.
Laboratory Courses in: Introductory Physics with Calculus and Modern Physics.

(d) Research: 1992-1993 (summers) **Physical Scientist Aid**, Naval Research Laboratory, Stennis Space Center, Mississippi.
Research topic: Acoustic study of fish migration.

1994 (summer) **Physical Scientist I**, Sverdrup Inc., Stennis Space Center, Mississippi.
Research topics: Ice movement in the Arctic ocean and Mediterranean current system using satellite imaging.

(e) Oceanographic Campaign: Participation aboard “KNORR” ship in the WOCE Oceanographic Campaign on leg A2.